# Theory of the nucleation kinetics of nematic droplets

Nimalasuriya, T.

*Award date:*
2004

TU/e technische universiteit eindhoven

Eindhoven University of Technology

Faculty of Physics
Polymer Physics Group
(PFY)
Building: N-laag
Postbus 513
5600 MB Eindhoven

# Theory of the Nucleation Kinetics of Nematic droplets

T. Nimalasuriya

Afstudeerdocent : Prof. dr. M.A.J. Michels

Begeleider : Dr. ir. P. van der Schoot

Datum : 18 februari 2004

## Abstract

Solutions of stiff polymers and other types of rod-like particle typically exhibit a first-order transition from the isotropic to the uniaxial nematic state. In a quench experiment, the nematic phase is formed either by nucleation and growth or by spinodal decomposition, depending on the quench depth. The nucleation of the nematic is unusual in that the nucleating droplets have shapes ranging from spherical to elongated and a director-field pattern ranging from homogeneous to bipolar. Experimental observations have shown a pronounced maximum in the nucleation rate in the biphasic region, leading to a near-zero rate of phase ordering.

In order to explain these observations, we set up a classical nucleation theory for the nematic, paying special attention to the contribution of the Laplace pressure to the nucleation barrier, which is a non-trivial function of the anisotropic interfacial and bulk elastic properties of the nucleating droplets. To investigate the free energy barrier, we evaluate the equilibrium shape and the director-field configuration of the droplets, taking into account elastic deformation of the director field and an anisotropic surface tension.In our description, we allow for a director field to transform continuously from a uniform to a bipolar configuration. We apply a recent kinetic theory for the linearised spinodal kinetics of hard rods to calculate the nucleation rates.

We calculate the barrier height for both rod-like particles and semi-flexible worms. We find that for deep quenches, leading to small critical nuclei, the Laplace pressure contribution cannot be ignored for rod-like particles. This effect is much less imminent for the semi-flexible worms. The height of the nucleation barrier and the nucleation rate with it, depends on the concentration quench, on the elastic properties of the droplets and on the Laplace pressure. We find that the pronounced maximum of the nucleation rate is caused by the critical slowing down of the nucleation dynamics near the spinodal. Finally, intended for future work, we look into an alternative route for calculating the free energy barrier of a nematic droplet using density functional theory for the case when classical nucleation theory fails.

# Chapter 1

# Introduction

## 1.1 Introduction

Nucleation occurs during a first order phase transition when a metastable state transforms into a stable state. In the case of a solution of, for example, rod-like particles, the first order transition occurs when a phase of randomly oriented rods, called an isotropic phase, begin to align in a particular direction and begin to form what is called a nematic liquid crystal. This is an activated process, a free energy barrier must be overcome in order to form nematic droplets or nuclei of critical size, beyond which the new phase grows spontaneously into a bulk nematic. The drive for this nucleation process for what is called a lyotropic liquid crystal is the increase of the concentration of particles, a concentration quench, beyond which the isotropic phase is stable. In contrast with a lyotropic liquid crystal, the thermotropic liquid crystal phase depends on temperature.

Whereas a metastable state relaxes by nucleation, an unstable state does so by spinodal decomposition. This second fundamental mechanism of phase separation occurs spontaneously, no free energy barriers need to be overcome. Spinodal decomposition can occur by applying a concentration quench deep into the region of coexisting isotropic and nematic phases. Spinodal decomposition involves the growth of density fluctuations of small amplitude that exceed a crit-

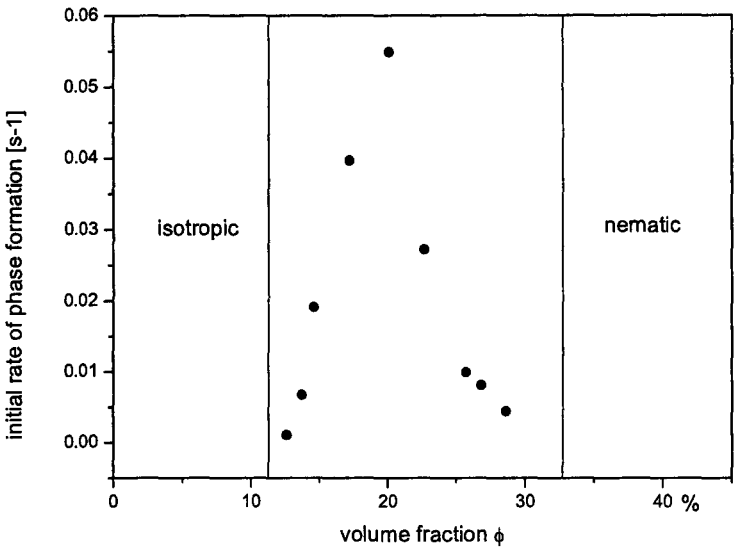


Figure 1.1: Nucleation rate of rodlike boehmite particles in cyclohexane, van Bruggen, Dhont, Lekkerkerker [2]

ical wavelength. Thus metastable systems relax by the activated growth of localised density fluctuations of large amplitude, whereas unstable systems do so by the spontaneous growth of long wavelength fluctuations of small amplitude. [1]

Experiments have shown that with increasing quench depth, nucleation rate shows a pronounced maximum, which has yet not been explained theoretically, see figure 1.1 [2]. Nucleation kinetics have been much investigated in the past. Russels adapted classical nucleation theory to describe crystal nucleation in hard sphere colloidal suspensions, assuming self-diffusivity mechanisms. [3] Dixit and Zukoski developed a pure kinetic approach based on particle gradient diffusivity as argued by Ackerson and Schätzel [4], calculating aggregation and dissociation rates for hard sphere suspensions. In these works a possible contribution to the Laplace pressure is neglected, despite the fact that the crystal nuclei in their calculations are small. Winters, Odijk en Van der Schoot have recently developed a theory for spinodal decomposition in a suspension of hard rods (hard meaning solely repulsive interaction between the rods) , where an unstable ori-

entation translation hybrid mode drives the nematic instability. Near the spinodal, the observed maximum can be explained by the critical slowing down of the hybrid mode [5].

In this thesis we investigate the nucleation of nematic liquid crystal droplets in the isotropic phase. Previous research has yielded the shape and structure of these droplets by minimising the free energy of these droplets at fixed volume [6], making it possible to now focus the attention on the dynamics of first order transition of liquid crystals.

The height of the energy barrier and nucleation rate depend on the free energy of the critical nucleus (the nucleus with the critical size at which the barrier appears). We have extended the expression for the free energy of nematic droplet formation which normally contains two terms, a negative contribution from a volume term and a positive contribution from a surface term. The total expression of the barrier consists of the surface anisotropy, depth of the concentration quench, elastic properties of the droplets and the Laplace pressure. We have found that when droplets are small, at large quench depth, the Laplace pressure cannot be neglected. The Laplace pressure inside a nematic droplet is significantly different than for a liquid droplet surrounded by vapour. For a liquid droplet with radius R and isotropic surface tension $\gamma$, the Laplace pressure can be written as $p = 2\gamma/R$. A nematic droplet has anisotropic surface tension and an internal structure subject to elastic deformation, making the Laplace pressure contribution a function of the anisotropic surface tension, the elastic constants for splay and bend deformation and the droplet volume.

We have applied a recent kinetic theory in order to calculate the lifetime of the nucleus. For small droplets approaching the particle size, the orientation and position of the individual rods need to be taken into account and the classical theory described above is no longer valid. We have investigated a density functional approach for nematic droplets in an isotropic phase for future research.

In the next section, a brief introduction of liquid crystals and the theoretical model of nematic droplets as described by [6], will be given. We describe the basic concepts of the so-called Classical Nucleation Theory, considering the nucleation barriers, the Laplace pressure and the

nucleation rate. For the conditions where the classical theory fails, we use a density functional approach which seems a useful alternative [7], and a brief outline will be given. In the final section of this chapter, we will regard possible applications.

## 1.2 Droplets of nematic liquid crystals

A liquid crystal consists of anisotropic colloidal particles, such as rods, semi-flexible worms or disc-shaped particles. There are two types of liquid crystal, thermotropic and lyotropic. In a thermotropic liquid crystal the phase is determined by the temperature, interaction between particles is mostly attractive and depending on the angle between the particles. Examples of thermotropic liquid crystals are elongated organic molecules such as MBBA and PAA. In a lyotropic liquid crystal, the type of liquid crystal we consider in this thesis, interaction between particles is repulsive as a result of excluded-volume interaction. The phase of a lyotropic liquid crystal depends on the concentration of anisotropic particles. As an example we will discuss a solution containing slender, monodisperse rods (rods with the same length) with only excluded-volume interaction (therefore called hard rods). Examples of hard rod particles are Tobacco Mosaic Virus (TMV), fd-virus and vanadium pentoxide. When the concentration of the rods is small, the rods are dispersed in random positions and orientations, this phase is called the isotropic phase. When the concentration is increased, the rods align in parallel with a common direction (called director) but their centers of mass have no long range positional order. This first order isotropic-nematic transition is entropically driven. Although the alignment of the particles reduces rotational entropy, translational entropy is increased because of an increased free volume per particle.

When the particle concentration is between the isotropic and the nematic, phase separation will occur by nucleation of nematic droplets, which will, because of the slightly higher density inside the nematic, grow and eventually sink to the bottom. These droplets can be regarded as floating in the solute, as sedimentation occurs very slowly, and therefore, the system can be considered as in quasi-equilibrium. It possible to capture these droplets on film using crossed

polarisers because of the birefringence caused by the aforementioned symmetry breaking. [6]

Tactoids are spindle-shaped nematic droplets and have been observed in dispersions of for example Tobacco Mosaic Virus (TMV), fd-virus, vanadium pentoxide, aluminium oxyhydroxide. Micrographs taken of these droplets using crossed polarisers suggest a bipolar director field (the local average orientation of the particles). In the bipolar configuration, the director field smoothly follows the contour of the droplet surface connecting two point defects at the poles of the droplet called boojums. [8]

Shape and director field configuration of tactoids were theoretically investigated by Prinsen and Van der Schoot [6] [9]. Optimal droplet shape was found by minimising the free energy of the droplets at fixed volume. The volume of the droplet is taken to be macroscopic on the scale of the particles, therefore neglecting finite-size effects on the stability of the nematic and on the degree of nematic order in the droplet. The free energy contains two contributions: an elastic free energy and a surface free energy. Competition between these two leads to the droplet shape and structure. The surface free energy consists of an isotropic surface tension and a contribution depending on the orientation of the director field at the surface. The angle between the director $\mathbf{n}$ and the normal to the surface $\mathbf{q}$ can be written as $(\mathbf{n} \cdot \mathbf{q})$. Assuming this angle to be small and the free energy invariant to the substitution $\mathbf{n} \rightarrow \mathbf{n}$ it can be expanded in terms of $(\mathbf{n} \cdot \mathbf{q})^2$. The constant term is the isotropic surface tension and in the surface free energy expression only the subsequent term is included. This leads to a Rapini-Papoular-like expression for the surface free energy $F_S$ [6]

$$F_S = \tau \int dA(1 + \omega(\mathbf{q} \cdot \mathbf{n})^2), \tag{1.1}$$

where $\tau$ and $\omega$ depend on the material properties of the liquid crystal. Integration is over the entire interfacial area $A$ of the droplet. Eq. 4.17 gives an accurate representation of theoretical predictions for the surface energy as function of the angle between the director and the normal on the surface. For lyotropic liquid crystals the particles have a preference to align parallel to the surface leading to $\omega > 0$. The surface tension $\tau$ is the interfacial tension between nematic droplet and the isotropic bulk phase, with typical values for lyotropic liquid crystals of $\tau \approx 10^{-5} Nm^{-1}$.

The surface anchoring strength $\omega$ is small if the interfacial tension is isotropic and large if it is strongly anisotropic, causing parallel alignment of the director field to the droplet surface to be favoured.

The elastic deformation energy depends on deviations of the homogeneous director field and is therefore a function of the director $\mathbf{n}$ and its derivatives $\nabla\mathbf{n}, \nabla^2\mathbf{n}$ etc. Assuming $L|\nabla\mathbf{n}| \ll 1$, $L^2|\nabla^2\mathbf{n}| \ll 1$, etc., and that $L^k|\nabla^k\mathbf{n}| \ll L^{k-1}|\nabla^{k-1}\mathbf{n}| \ll 1$, with L the droplet length, the elastic free energy can be expanded in a Taylor series in terms of $\nabla\mathbf{n}$. The elastic free energy has to be invariant with regard to the substitution $\mathbf{n} \rightarrow \mathbf{n}$, and is scalar invariant with respect to an orthogonal transformation of the basis. The Frank-Leslie elastic free energy $F_E$ (after considerable simplification) can then be written as [6]

$$F_E = \frac{1}{2}\int dV[K_{11}(\nabla \cdot \mathbf{n}) + K_{33}(\mathbf{n} \times (\nabla \times \mathbf{n}))], \tag{1.2}$$

where Frank elastic constants $K_{11}$ and $K_{33}$ represent splay and bend deformation of a bulk nematic, and $\mathbf{n}$ represents the director. Other elastic constants such as the twist constant $K_{22}$ and saddle splay $K_{24}$, have been neglected as we ignore the twisted bipolar configuration, and we absorb the influence of $K_{24}$, which represents the so-called saddle-divergence and can be written as a surface integral using Gauss'theorem, into $K_{11}$. The integration is over the entire volume of the droplet.

The value of the elastic constants depend on the type of liquid crystal, the temperature, the concentration of the anisotropic particles and the solvent. For a lyotropic liquid crystal solution of monodisperse, rigid rod-like particles of Tobacco Mosaic Virus, $K_{11} \approx 10^{-12} - 10^{-10}N$, the ratio of the elastic constants for splay and bend $\gamma_{33} \equiv K_{33}/K_{11} \approx 9 - 17$. Theoretical predictions indicate that $5 \lesssim \gamma_{33} \lesssim 10$ for hard rods (found to agree with data for TMV), in this study this is taken to be 10. For semi-flexible worms, like the lyotropic liquid crystal PBG (poly-$\gamma$-benzyl-glutamate), $\gamma_{33} \approx 1$ and in this study this value is chosen for worm-like particles, although it does depend on a intricate combination of persistence length, density and particle length. [6]

Applying geometric arguments, an estimate of the shape and structure of the droplets can be made. The elastic free energy is proportional to $V^{1/3}$ whereas the surface free energy is

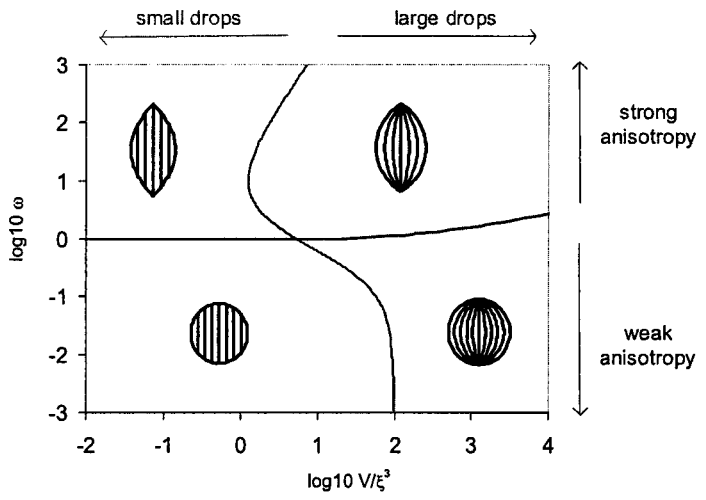


Figure 1.2: scaling regimes with different droplet types

proportional to $V^{2/3}$, with $V$ the droplet volume. So for large droplets the surface free energy wins out leading to the elongated particles to be aligned parallel to the surface resulting in a bipolar director field, where the director field goes from one point of the droplet to the other. For small droplets the elastic free energy wins out, so there the director field is uniform. For large $\omega$, the droplets are elongated and for small $\omega$ the droplets are spherical. This is clarified in the phase diagram, see figure 1.2, also containing schematic representation of extreme droplet types: elongated bipolar (tactoid), spherical bipolar, elongated homogeneous, spherical homogeneous. In reality, the transition between the various droplet types is continuous. With increasing droplet size the director field crosses over smoothly from a homogeneous to a bipolar configuration. Virtual boojums [10], points where the director field comes together, move in from infinity towards the poles on the surface of the droplet.

## 1.3 Classical nucleation theory

Classical Nucleation Theory ($CNT$) is based on the assumption that droplets originating from the nucleation of a bulk nematic from the isotropic phase can be described with a macroscopic theory even if they are very small. Droplets have a well defined volume, with the nematic phase inside and the isotropic phase outside. The free energy of nematic droplet formation can in general be described as the sum of two terms: a negative contribution from the bulk free energy, proportional to the droplet volume and a positive contribution from the surface free energy, proportional to the droplet surface area. Hence,

$$\Delta G = \rho \Delta \mu V + \tau V^{2/3} + ..., \tag{1.3}$$

where $\Delta G$ is the Gibbs free energy, $\rho$ is the density of the phase inside the droplet, $\Delta\mu$ is the chemical potential difference between the nematic and isotropic phase, $\tau$ is the isotropic surface tension and $V$ is the droplet volume. For a metastable state, $\Delta\mu$ is negative, therefore an increase in volume eventually results in an energy barrier that can be crossed so that the isotropic nematic transition can take place. The droplet size and the free energy that forms the barrier to nucleation can then be calculated as a function of the concentration increase known as concentration quench depth.

In order to maintain mechanical equilibrium during droplet formation, the droplet pressure increases according to a generalised Laplace equation: [11]

$$p_n = p + \frac{\partial F}{\partial V_n}, \tag{1.4}$$

where $V_n$ is the droplet volume and $p_n$ represents the osmotic pressure within the droplet and $p$ outside . We use the Laplace pressure to take the droplet curvature into account when calculating the work for droplet formation. Free energy depends on the elastic and the surface energies, the surface anisotropy and the volume. We will proceed in the chapter two by inserting the Laplace equation into the expression for the work needed to form a droplet and then expand to first order so that we obtain an expression for the nucleation barrier for nematic droplets in an isotropic phase.

The nucleation rate is proportional to the thermodynamic probability of having a fluctuation leading to a critical cluster and a dynamical factor $\mathcal{A}$ describing the rate at which the cluster grows [12]

$$I_s = \mathcal{A} \exp[-\beta \Delta G_{n_*}], \tag{1.5}$$

where $\beta \Delta G_{n_*}$ is the dimensionless height of the nucleation barrier, which is the minimum reversible work for cluster formation. We calculate the barrier height by minimising the droplet free energy with respect to the droplet volume. $\mathcal{A}$ contains the particle number, the so-called Zeldovich factor, which signifies the fact that not all particles at the top of the nucleation barrier end up in the nematic phase but can recross and end up in the isotropic phase, and the rate at which a critical nucleus grows. This attachment rate consists of the number of particles available at the surface of the critical nucleus, $\sim n_*^{2/3}$, and a transition rate of these particles to become part of the nucleus. This transition rate is proportional to $D/\ell$ where D is a diffusion coefficient and $\ell$ a typical distance over which the diffusion takes place. [13] We proceed in chapter four by applying a recent kinetic theory in order to identify this diffusion coefficient and to explain the sharp maximum observed in nucleation rate with increasing quench depth of figure 1.1.

## 1.4 Density functional approach

Classical Nucleation Theory fails as the spinodal is approached. CNT predicts a finite barrier to nucleation while the main property of the spinodal is the vanishing of this barrier as fluid passes from a thermodynamically metastable state to an unstable one. [14]. As a macroscopic theory CNT also fails when the droplet size begins to approach the particle size. This occurs after deep quenches because the droplet size is inversely proportional to the quench depth. Macroscopic theory must therefore be replaced with a microscopic theory such as density functional theory. This theory makes no assumptions about the homogeneity of the nucleus and therefore, no division of the free energy in a volume and surface term is needed.

Density-functional theory considers thermodynamic potentials of an inhomogeneous system

as functionals of the inhomogeneous density $\rho(\mathbf{x})$, of which $\mathbf{x}$ can denote both position and orientation and we later replace with $(\mathbf{r}, \mathbf{u})$. The Helmholtz free energy can be written as [7]

$$F[\rho(\mathbf{x})] = F^{id}[\rho(\mathbf{x})] + F^{ex}[\rho(\mathbf{x})] \tag{1.6}$$

This expression contains an ideal entropy part

$$F^{id}[\rho(\mathbf{x})] = kT \int \rho(\mathbf{x})[\ln(\rho(\mathbf{x}) - 1)]dx \tag{1.7}$$

The second term in eq. 1.6 represents an excess free energy as a result of interaction between particles.

Doi and Kuzuu calculated the free energy of coexisting isotropic and nematic phases, separated by a plane interface in the x-y plane.

$$F^{ex}[\rho(\mathbf{r},\mathbf{u})] = \frac{1}{2} \int \rho(\mathbf{r}, \mathbf{u})\rho(\mathbf{r}', \mathbf{u}')\delta(\mathbf{r} - \mathbf{r}'; \mathbf{u}\mathbf{u}')d^2\mathbf{u}'d^3\mathbf{r}'d^2\mathbf{u}d^3\mathbf{r}, \tag{1.8}$$

where $\delta$ accounts for the excluded volume interaction (particles cannot interpenetrate each other). In their excess free energy term they identify an excluded volume term and a spatial inhomogeneity term. [15] In order to calculate the free energy they use Onsager's trial function for the orientational profile [16]

$$f(\mathbf{u}) = \frac{\alpha}{4\pi \sinh(\alpha)} \cosh(\mathbf{u} \cdot \mathbf{n}), \tag{1.9}$$

where $\alpha$ is a variational parameter and $\theta$ the angle between the unit vector parallel to the particle and the director. They extend the trial function for the continuous transition from the isotropic to the nematic by constructing a density profile $\rho$ that is both dependent on orientation and position. We investigate the possibility of applying the density profile of a spherical droplet in chapter five.

## 1.5 Technology assessment

Nematic droplets can be found in everyday life, for example in technology like PDLCs (Polymer Dispersed Liquid Crystals) but also in biology and in medicine.

PDLCs operate on the principle of electrically controlled light scattering. They consist of liquid crystal droplets surrounded by a polymer mixture sandwiched between two pieced of conducting glass. When no electric field is applied the liquid crystal droplets are randomly oriented creating an opaque state, but when applied, the liquid crystals align parallel to the electric field and light passes through, creating a transparent state. The droplet size is important, because the electric field needed to align the droplets is inversely proportional to the droplet size. A useful application for this principle is a window, which with the flip of a switch changes from opaque to clear. Nucleation theory is of great use to the production and development of PDLC materials. During the production process, nematic droplets nucleate inside a polymeric matrix. [17] Material properties are determined by droplet type and size, so it is of great interest to the industry to have insight in these processes.

Another example of nematic droplets can be found in biology. The protein actin is present in may different cell types and plays a variety of roles in the cytoskeleton. The elementary building block is the protein g-actin (Globular actin), a single chain of approximately 375 amino acids. g-actin units can assemble into a long string called f-actin (filamentous actin), which consists of two strands forming a coil, which is approximately 8 nm wide. [18] Actin filaments have a relatively simple structure and it is possible to make images of single filaments in a solution. It is therefore an ideal system for biophysical research of for example semi-flexible polymer dynamics. [19] Tactoids have been observed in the concentrated gels of actin filaments (f-actin). Microscopy shows these stable tactoids of densely packed f-actin to be of various size of order $10\mu m$. It is assumed that the formation is driven primarily by the excluded-volume effects. [20]

One example of tactoids in medicine is a pathological anomaly of the human red blood cell. Human red blood cells are flat round disks without nuclei, indented in the middle on both sides. Their greatest thickness at the edge is $2\mu m$. The main function of the red blood cells is the transport of oxygen and is facilitated by its characteristic shape, for the diffusion area is large and the diffusion distance small. Because of the shape of the cells it is easier to be reversibly deformed in order to pass through narrow curved capillaries. The elasticity of the cell reduced in pathological form of red blood cells, such as sickle cells. The loss of elasticity causes the cells

to be retained in the meshwork of the spleen where they are destoyed, causing what is known as sickle cell anemia. [21]

In case of sickle cell anemia, a point mutation arises in the amino acid sequence of the cell, resulting in the synthesis of unusual proteins at the surface of the molecule of hemoglobin. The hemoglobin polymerises into long 210 $\AA$ diameter fibres that result in the nucleation of tactoids. [22] The higher the concentration of tactoids, the quicker the crystallisation when exposed to a low oxygen environment. Tactoids tend to: 1) decrease hemoglobin solubility, 2) change the shape of the red blood cell, 3) decrease deformability of the red cell. These factors act together to change the red cell shape from a biconcave disc to a sickle-shape. With recurrent exposure to low oxygen in the blood, the red blood cells tend to acquire a sickle shape permanently causing serious pathological effects in the patient.

## 1.6 Thesis overview

In the next chapter we give a review of the free energy of nematic droplets with the boojums residing outside of the droplet. We describe the free energy of the droplet using scaling theory as calculated by [8] and distinguish droplet types belonging to five different regimes [6]. For each of these regimes we calculate the nucleation barrier. We adapt the expression for the nucleation barrier by adding a contribution of the Laplace pressure.

We then proceed by calculating these barriers for both rigid rod-like particles and worms. We distinguish between both particles by finding scaling relations describing the parameters for both rods and worms and then examine the different outcomes. Finally we calculate the limit of classical nucleation, so that we know when the classical theory needs to be replaced with DFT.

We then study the nucleation kinetics of rigid rods by first calculating the prefactor of the nucleation rate. For this we combine a general theory for liquids with a recent kinetic theory for hard rods. [5] Finally we calculate the nucleation rate, for which we also use the barrier heights calculated in the previous chapter.

We then investigate an alternative route for the use of density-functional theory for the calculation of the free energy of nematic droplets, intended for future work.

# Chapter 2

# The nucleation barrier of a nematic droplet

## 2.1 Introduction

We begin our study of the nucleation of nematic droplets with a review of the free energy of nematic droplets with the boojums, residing on the outside of the droplets, as described in the first chapter the boojums are then called virtual boojums. As described in the previous chapter, the free energy can be described by two functionals, an elastic free energy functional, which is associated with the deformation of the director field, and an anisotropic interfacial free energy functional. We analyse these free energy functionals using a scaling analysis in order to obtain a qualitative picture of the equilibrium droplet shapes and structures based on the asymptotic limits of the free energy. The free energy has been calculated in detail by Prinsen [6] and we use these to calculate the energy barrier that must be overcome in order for nucleation to occur. In the case of nematic droplets the calculation of the nucleation barrier is complicated as it depends on the anchoring strength, on the Frank elasticity of the critical nuclei and on the Laplace pressure. The Laplace pressure, though generally ignored when the nucleation of crystalline or incompressible fluid phases is investigated [3], plays an important part in the calculation of the

barriers of small droplets and has as far as we are aware never been applied to nematic liquid crystals before. We point out the significance of this Laplace pressure in the following chapter.

## 2.2 Free energy of a nematic droplet with a transitional director field

We consider a nematic droplet of volume V, nucleated in the isotropic phase. If the volume of the droplet is macroscopic on the scale of the particles, we need not take into account the internal (grainy) structure of the droplet. As explained in the previous chapter, the free energy $F$ of a nematic tactoid can then be described as the sum of the free energy cost of the deformation of the director field $F_E$ and that of the presence of the interface which separates the nematic from the isotropic phase $F_S$,

$$F = \tau \int dA(1 + \omega(\mathbf{q} \cdot \mathbf{n})^2) + \frac{1}{2} \int dV[K_1(\nabla \cdot \mathbf{n}) + K_3(\mathbf{n} \times (\nabla \times \mathbf{n}))], \tag{2.1}$$

where $\mathbf{n}$ is the director, $\mathbf{q}$ is the unit vector perpendicular to the interface of the droplet, $K_{11}$ and $K_{33}$ are the Frank elastic constants for the splay and bend deformation modes, $\omega$ is the anchoring strength and $\tau$ is the isotropic surface tension. Other elastic constants have been omitted for reasons already explained. There are three dimensionless parameters that determine the optimal shape and structure, namely the anchoring strength $\omega$, the ratio of the elastic constants $\gamma_{33} \equiv K_{33}/K_{11}$ and the dimensionless volume $v \equiv V/\xi^3$, with the so-called extrapolation length $\xi \equiv K_{11}/\tau\omega$ [23]. The extrapolation length $\xi$ measures the scale below which the director field resists deformation by the coupling to the interface. The equilibrium shape and director field can be found by optimising the free energy functional in eq. 2.1. The shapes, chosen to resemble droplet shapes found in experiments, are circle sections rotated about their chord, producing both droplet shapes ranging from elongated to spherical depending on the position of the chord. The director field is determined by a collection of circle sections intersecting at two points that are at $\tilde{R} > R$ distance to the center of the droplet on the rotation axis of the droplet. $\tilde{R}$ is the distance from the center of the droplet to either of the point defects.

The point defects where the field lines intersect are outside the droplet and are therefore called (as was done so by Rudnick and Bruinsma [10]) virtual defects or virtual boojums. The director field of these droplets are therefore so-called quasi bipolar, as the director field can be truly homogeneous for very small droplets or truly bipolar for very large ones for these limits only. The free energy depends on the ratio $R/\tilde{R}$, $\kappa$, and the inverse aspect ratio of the droplet, $\varepsilon$, which are used next for the scaling estimates.

## 2.3 Scaling theory

In order to find out the different regimes for the different droplet types, a scaling estimate, based on the work of Prinsen and Van der Schoot, [8] is made of the dimensionless free energy $\tilde{F}$. The free energy is made dimensionless by dividing it by the surface tension $\tau$ and by dividing it by $V^{2/3}$, so the dimensionless free energy can be written as $\tilde{F} \equiv F/V^{2/3}\tau$. Let $R$ be the major axis and $r$ be the minor axis of the droplet. The inverse aspect ratio $\varepsilon$ can now be expressed as $r/R$. For elongated droplets $\varepsilon \ll 1$, and for spherical droplets $\varepsilon \approx 1$. The ratio $R/\tilde{R}$ can be seen as the measure for the radius of curvature of the director field, as for $R/\tilde{R} \ll 1$ the director-field is homogeneous and for $R/\tilde{R} \approx 1$ the director-field is bipolar.

The volume $V$ of the droplet scales as $r^2R$ and the surface area as $rR$. The surface contribution is equal to the surface tension $\tau$ times the area $A \approx Rr$, times a correction that penalises the non-tangential alignment of the director field. This correction involves a surface average of $\omega(\mathbf{q}\cdot\mathbf{n})^2$ that can be shown to scale as $\omega r^2R^2(R^{-2} - \tilde{R}^{-2})^2$[6]. The limits of the director field (truly bipolar and truly homogeneous) can be deduced from these scaling estimates as for a truly homogeneous director field $R/\tilde{R} \to 0$, and for a truly bipolar director field $R/\tilde{R} \to 1$. By geometry, the radius of curvature of a bend deformation scales as $\tilde{R}^2/r$ so that the contribution of the bend deformation becomes $K_{33}(R^2)(\tilde{R}^2/r)^{-2} = K_{33}r^4R/\tilde{R}^4$. The radius of curvature of splay deformation is $\tilde{R}^2/R$ so that the deformation becomes $K_{11}(r^2R)(\tilde{R}^2/R)^{-2} = K_{11}r^2R^3/\tilde{R}^4$. Comparing the contribution of the bend deformation with that of the splay deformation shows the latter to be larger or of the same order of magnitude as the bend contribution, making it

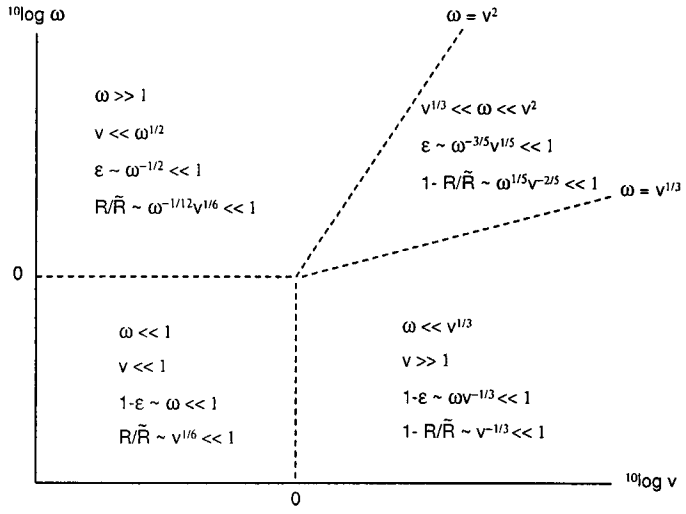


Figure 2.1: scaling estimates of extreme droplettypes and their corresponding regimes.[6]

therefore possible to ignore the bend contribution [6]. After insertion of the surface free energy and the elastic bend deformation energy into expression 2.1, the scaled dimensionless free energy can be written as

$$\tilde{F} \equiv \omega v^{-1/3}\kappa^4\varepsilon^{4/3} + \varepsilon^{-1/3} + \omega\varepsilon^{5/3}(1-\kappa^2)^2, \tag{2.2}$$

where $v$ is the scaled droplet volume, $\kappa \equiv R/\tilde{R}$ is a measure for the radius of curvature of the director-field of the droplet and $\varepsilon \equiv r/R$ the inverse aspect ratio of the droplet. Optimal values for $\varepsilon$ and $\kappa$ for the different droplet types are found by minimising eq. 2.2 with respect to $\varepsilon$ and $\kappa$ and solving the obtained equations. For elongated droplets, $\varepsilon \ll 1$, the following scaling relations have been found, $\varepsilon \approx \kappa^6 v^{-1}(1-\kappa^2)^{-3}$ and $\omega v^{-2} \approx \kappa^{-12}(1-\kappa^2)^5$. For a homogeneous director field, $\kappa \ll 1$, and therefore $v \ll \omega^{1/2}$ leading to $\kappa \approx \omega^{-1/12}v^{1/6}$ and $\varepsilon \approx \omega^{-1/2}$. For a bipolar director field, $\kappa \approx 1$, and therefore $v \gg \omega^{1/2}$ leading to $1-\kappa \approx \omega^{1/5}v^{-2/5}$ and $\varepsilon \approx \omega^{-3/5}v^{1/5}$. As $\varepsilon \ll 1$ the latter can be written as $\omega v^{-1/3} \gg 1$. For spherical droplets, $\varepsilon = 1$, the following relations have been found by minimising 2.2, with respect to $\kappa$ to give $\kappa^{-2}(1-\kappa^2) = v^{-1/3}$, leading to $\kappa \approx v^{1/6}$ for $v \ll 1$ and $1-\kappa \approx v^{-1/3}$ for $v \gg 1$. [6] An overview of the different scaling estimates and their corresponding regimes can be found in Figure 2.1 [6].

As can be seen from figure 2.1, there are two scaling regimes for $\omega \ll 1$, namely $v \ll 1$

and $v \gg 1$, and three for $\omega \gg 1$, namely $v \ll \omega^{1/2}$, $\omega^{1/2} \ll v \ll \omega^3$ and $v \gg \omega^3$. The asymptotic limits of the dimensionless free energies of the various droplet types belonging to these regimes are listed in table 2.1 For each regime corresponding to a particular droplet type

| **droplet type** | **asymptotic limit** | **scaling regime** | **droplet free energy** |
|---|---|---|---|
| homogeneous spherical | $\varepsilon \approx 1$ , $\kappa \ll 1$ | $v \ll 1$ , $\omega \ll 1$ | $\tilde{\tau} v^{2/3}$ |
| bipolar spherical | $\varepsilon \approx 1$ , $\kappa \approx 1$ | $v \gg 1$ , $\omega \ll v^{1/3}$ | $\tilde{\tau} v^{2/3} + \tilde{\tau} v^{1/3}$ |
| homogeneous elongated | $\varepsilon \ll 1$ , $\kappa \ll 1$ | $v \ll \omega^{1/2}$ , $\omega \gg 1$ | $\tilde{\tau} v^{2/3}$ |
| bipolar elongated | $\varepsilon \ll 1$ , $\kappa \approx 1$ | $v^{1/3} \ll \omega \ll v^2$ | $\tilde{\tau} v^{3/5}$ |

Table 2.1: asymptotic limits corresponding to the droplet type, the scaling regimes and dimensionless free energy without numerical prefactor, as calculated by [6]. For more detailed expressions for the free energy, see appendix A.

(in the asymptotic limit) the dimensionless free energy has also been calculated exactly, i.e. inclusive of the numerical prefactors. [6] The dimensionless free energy $\tilde{F}$, depending on $\omega$ and the ratio of elastic constants $\gamma_{33}$, we inserted into the expression for the nucleation barrier which we derive in the next section.

## 2.4 The Laplace pressure

We begin with analysing the Gibbs free energy of the formation of a critical nucleus (the nucleus for which the Gibbs free energy passes through a maximum). The theory applied is described by Kaschiev, who investigated the excess energy of a nucleus, which, combined with the difference between chemical potentials, makes up the work for a homogeneous formation of a nucleus. [11]

A droplet can be described as a nucleus consisting of $n$ particles. The Gibbs free energy of an $n$-sized nucleus takes into account the energy changes in the system that accompany the formation of a nucleus and can be described as

$$\Delta G(n) = n\mu_{nem} + G_{ex}, \tag{2.3}$$

where $n\mu_{nem}$ is the Gibbs free energy the nucleus would have had were it a a part of the bulk nematic phase and $G_{ex}$ is the nucleus excess energy. The nucleus excess energy accounts for three effects: the existence of an interface between the nematic nucleus and the isotropic bulk phase, the changed pressure in the volume of the nucleus and the differences in chemical potential of the nucleus and bulk phase. The Gibbs free energy representing the work for the formation of a nucleus can be written as [11]

$$\beta\Delta G = \rho\Delta\mu V_n + G_{ex}, \tag{2.4}$$

where the chemical potential difference between isotropic and nematic bulk phases is written as $\Delta\mu = (\mu_{iso} - \mu_{nem})$, $V_n$ is the droplet volume and $\rho$ the density of the phase inside the drop. After applying thermodynamic relations, this can be expressed as [11]

$$G_{ex} = F(V_n) - (p_n - p)V_n + \int_p^{p_n} V_n(P)dP \quad , \tag{2.5}$$

where $F$ is the total free energy of the nucleus as described by eq. 2.1, $p_n$ is the osmotic pressure inside the nucleus, $p$ is the osmotic pressure of the bulk isotropic phase. The advantage of this expression for the excess energy is that it is not necessary to know the value of $\mu_{n,nem}$ of the nucleus. For an incompressible fluid, only the first term survives as the third term of 2.5 then cancels out the second term. The nematic droplet however is osmotically compressible, therefore giving rise to a change in pressure in the volume after droplet formation. In order to maintain mechanical equilibrium the droplet pressure increases

$$p_n = p + \frac{\partial F}{\partial V_n} \tag{2.6}$$

Invoking the equation of state for bulk hard-rod nematics (valid only in the Gaussian limit) [24] as described by Onsager [16]

$$V_n(p_n) = 3nkT/p_n \tag{2.7}$$

Now the cluster excess energy $G_{ex}$ can be calculated by combining both eq. 2.6 and eq. 2.5 and by applying a Taylor expansion with respect to $p_n/p$ to the first order

$$G_{ex} = F + \frac{1}{2}pV_n(\frac{F'}{p})^2 + ..., \tag{2.8}$$

where $F' = \partial F/\partial V_n$. Inserting this into the expression for the total free energy of droplet formation 2.3, the dimensionless expression for the Gibbs free energy becomes

$$\beta\Delta G = \beta F + \frac{1}{2}\beta p V_n (\frac{F'}{p})^2 + \rho\beta\Delta\mu V_n, \tag{2.9}$$

where the second term on the right hand side is the Laplace pressure contribution. It is this contribution that accounts for the effect of a curved surface (the droplet), as the first term $\Delta\mu$ represents the difference in chemical potential between the bulk phase of the nematic and isotropic phase and therefore accounts for a flat interface between the nematic and isotropic.

By minimising eq. 2.9 with respect to the dimensionless volume $v$, we find the dimensionless volume of the critical nucleus $v_*$, and by inserting this back into eq. 2.9 we find the nucleation barrier height of the droplet approximated to the first order. We now present the five barrier heights and corresponding critical droplet volume for the asymptotic limits of the free energy of eq. 2.1 as calculated by Prinsen [6].

1. Homogeneous elongated droplets, $\omega \gg 1, v \ll \omega^{1/2}$

$$\beta\Delta G_* \cong 32\left(\frac{4\pi}{15}\right)\omega_1^3\tilde{\tau}^3\tilde{\rho}^{-2}\frac{1}{|\beta\Delta\mu|^2} + 32\left(\frac{4\pi}{15}\right)\omega_1^3\tilde{\tau}^2\tilde{\rho}^{-1}\frac{1}{|\beta\Delta\mu|}\mathcal{L} \tag{2.10}$$

2. Homogeneous spherical droplets, $\omega \ll 1, v \ll 1$

$$\beta\Delta G_* \cong 32\left(\frac{4\pi}{15}\right)\omega_1^3\tilde{\tau}^3\tilde{\rho}^{-2}\frac{1}{|\beta\Delta\mu|^2} + 32\left(\frac{4\pi}{15}\right)\omega_1^3\tilde{\tau}^2\tilde{\rho}^{-1}\frac{1}{|\beta\Delta\mu|}\mathcal{L} \tag{2.11}$$

3. Bipolar elongated droplets, $\omega \gg 1, v^{1/3} \ll \omega \ll v^2$

$$\begin{aligned}&\beta\Delta G_* \cong \tfrac{8}{3}\pi\left(\tfrac{8}{15}\right)^{3/2}\omega_2^{5/2}\tilde{\tau}^{5/2}\tilde{\rho}^{-3/2}\tfrac{1}{|\beta\Delta\mu|^{3/2}} + \\ &4\sqrt{2}\pi\left(\tfrac{8}{15}\right)^{3/2}\omega_2^{5/2}\tilde{\tau}^{3/2}\tilde{\rho}^{-1/2}\tfrac{1}{|\beta\Delta\mu|^{1/2}}\mathcal{L}\end{aligned} \tag{2.12}$$

4. Bipolar spherical droplets, $\omega \gg 1, \omega \ll v^{1/3}$

$$\begin{aligned}&\beta\Delta G_* \cong 4\left(\tfrac{4\pi}{3}\right)\tilde{\tau}^{3/2}\tilde{\rho}^{-1/2}\tfrac{1}{|\beta\Delta\mu|^{1/2}}(\gamma_4\omega)^{3/2} + 9\left(\tfrac{4\pi}{3}\right)\tilde{\tau}^2\tilde{\rho}^{-1}\tfrac{1}{|\beta\Delta\mu|}(\gamma_4\omega)^{1/2} + \\ &4\left(\tfrac{4\pi}{3}\right)\tilde{\tau}^{3/2}\tilde{\rho}^{-1/2}\tfrac{1}{|\beta\Delta\mu|^{1/2}}(\gamma_4\omega)^{1/2}\mathcal{L} + \\ &6\left(\tfrac{4\pi}{3}\right)\tilde{\tau}^2\tilde{\rho}^{-1}\tfrac{1}{|\beta\Delta\mu|}\mathcal{L} + \\ &2\left(\tfrac{4\pi}{3}\right)\tilde{\tau}(\gamma_4\omega)\mathcal{L},\end{aligned} \tag{2.13}$$

5. Bipolar spherical droplets, $\omega \ll 1, \omega \ll v^{1/3}$

$$\beta\Delta G_* \cong 4\left(\frac{4\pi}{3}\right)\tilde{\tau}^3\tilde{\rho}^{-2}\frac{1}{|\beta\Delta\mu|^2}+6(\gamma_4\omega)\left(\frac{4\pi}{3}\right)\tilde{\tau}^2\tilde{\rho}^{-1}\frac{1}{|\beta\Delta\mu|}+4\left(\frac{4\pi}{3}\right)\tilde{\tau}^2\tilde{\rho}^{-1}\frac{1}{|\beta\Delta\mu|}\mathcal{L} \quad (2.14)$$

As can be seen from 2.17 till 2.14 the first term of the nucleation barrier corresponds to the classical vapour nucleation where $\beta\Delta G \sim \tau^3\beta\Delta\mu^{-2}$ and the second (following) term with the Laplace correction for the droplet curvature.

| **droplet type** | **critical droplet volume $v_*$** |
|---|---|
| homogeneous spherical | $\left(\frac{4\pi}{3}\right)\omega_3^3\tilde{\tau}^3\tilde{\rho}^{-3}\frac{1}{\lvert\beta\Delta\mu\rvert^3}(1+\sqrt{1+\frac{2}{3}\mathcal{L}\frac{\tilde{\rho}\lvert\beta\Delta\mu\rvert}{\tilde{\tau}}})^3$ |
| bipolar spherical | $\left(\frac{4\pi}{3}\right)\tilde{\tau}^3\tilde{\rho}^{-3}\frac{1}{\lvert\beta\Delta\mu\rvert^3}(1+\sqrt{1+\frac{2}{3}\tilde{\mathcal{L}}\frac{\tilde{\rho}\lvert\beta\Delta\mu\rvert}{\tilde{\tau}}})^3$ |
| homogeneous elongated | $8\left(\frac{4\pi}{3}\right)\omega_1^3\tilde{\tau}^3 r\tilde{h}o^{-3}\frac{1}{\lvert\beta\Delta\mu\rvert^3}(1+\sqrt{1+\frac{2}{3}\mathcal{L}\frac{\tilde{\rho}\lvert\beta\Delta\mu\rvert}{\tilde{\tau}}})^3$ |
| bipolar elongated | $\pi\left(\frac{15}{8}\right)^{3/2}\omega_2^{5/2}\tilde{\tau}^{5/2}r\tilde{h}o^{-5/2}\frac{1}{\lvert\beta\Delta\mu\rvert^3}(1+\sqrt{1+\frac{2}{3}\mathcal{L}\frac{\tilde{\rho}\lvert\beta\Delta\mu\rvert}{\tilde{\tau}}})^{5/2}$ |

Table 2.2: critical droplet volumes for a solution containing rod-like particles

where the Laplace pressure correction $\mathcal{L} \equiv \tau(p\,\xi)^{-1}$, $\tilde{\mathcal{L}} = 2/3\mathcal{L}+\gamma_4\omega$, $\tilde{\tau} \equiv \beta\xi^2\tau$, $\tilde{\rho} \equiv \xi^3\rho$, $\gamma_4 \equiv (1+(12-\pi^2)/16\gamma_{33})$, $\omega_1 \equiv \omega^{1/6}(1+(21\omega)^{-1})$, $\omega_2 \equiv \omega^{1/5}$ and $\omega_3 \equiv (1+(1/3)\omega-(\pi^2/36(\pi^2-8))\omega^2)$ and $\beta\Delta\mu$ represents the concentration quench depth as it is related to the number of particles added to the system [24]. Again, the the first term of the droplet volume in 2.3 corresponds to the classical vapour nucleation where $v_* \sim \tau^3\beta\Delta\mu^{-3}$ and the second (following) term with the Laplace correction for the droplet curvature.

For worms, the equation of state as used for eq. 2.8 is incorrect, a different expression is needed for the equation of state and subsequently the work of the formation of a nucleus, the droplet volume and the nucleation barrier. The equation of state for semi-flexible worms can be written as [7]

$$V_n = 2^{-1/3}LP^{-1/5}D^{2/5}p_n^{-3/5}n(kT)^{3/5}, \quad (2.15)$$

where $L$ is the contour length, $P$ is the persistence length, $D$ is the diameter and $V_n$ is the volume of the nucleus. This leads to the following expression for the total free energy of droplet

formation

$$\beta\Delta G = \beta F + \frac{3}{10}\beta pV(\frac{F'}{p})^2 + \rho\beta\Delta\mu V, \tag{2.16}$$

The Laplace correction is smaller for worms than for rods. This could be explained by the fact that the semi-flexible worms are less resistant to the droplet curvature. Next we give the results for the calculations of the critical droplet volume and the barrier height.

1. Homogeneous elongated droplets, $\omega \gg 1, v \ll \omega^{1/2}$

$$\beta\Delta G_* \cong 32\left(\frac{4\pi}{15}\right)\omega_1^3\tilde{\tau}^3\tilde{\rho}^{-2}\frac{1}{|\beta\Delta\mu|^2} + \frac{96}{5}\left(\frac{4\pi}{15}\right)\omega_1^3\tilde{\tau}^2\tilde{\rho}^{-1}\frac{1}{|\beta\Delta\mu|}\mathcal{L} \tag{2.17}$$

2. Homogeneous spherical droplets, $\omega \ll 1, v \ll 1$

$$\beta\Delta G_* \cong 32\left(\frac{4\pi}{15}\right)\omega_1^3\tilde{\tau}^3\tilde{\rho}^{-2}\frac{1}{|\beta\Delta\mu|^2} + \frac{12}{5}\left(\frac{4\pi}{15}\right)\omega_1^3\tilde{\tau}^2\tilde{\rho}^{-1}\frac{1}{|\beta\Delta\mu|}\mathcal{L} \tag{2.18}$$

3. Bipolar elongated droplets, $\omega \gg 1, v^{1/3} \ll \omega \ll v^2$

$$\begin{aligned}&\beta\Delta G_* \cong \tfrac{8}{3}\pi\left(\tfrac{8}{15}\right)^{3/2}\omega_2^{5/2}\tilde{\tau}^{5/2}\tilde{\rho}^{-3/2}\tfrac{1}{|\beta\Delta\mu|^{3/2}} + \\ &\tfrac{12}{5}\sqrt{2}\pi\left(\tfrac{8}{15}\right)^{3/2}\omega_2^{5/2}\tilde{\tau}^{3/2}\tilde{\rho}^{-1/2}\tfrac{1}{|\beta\Delta\mu|^{1/2}}\mathcal{L}\end{aligned} \tag{2.19}$$

4. Bipolar spherical droplets, $\omega \gg 1, \omega \ll v^{1/3}$

$$\begin{aligned}&\beta\Delta G_* \cong 4\left(\tfrac{4\pi}{3}\right)\tilde{\tau}^{3/2}\tilde{\rho}^{-1/2}\tfrac{1}{|\beta\Delta\mu|^{1/2}}(\gamma_4\omega)^{3/2} + 9\left(\tfrac{4\pi}{3}\right)\tilde{\tau}^2\tilde{\rho}^{-1}\tfrac{1}{|\beta\Delta\mu|}(\gamma_4\omega)^{1/2} + \\ &\tfrac{12}{5}\left(\tfrac{4\pi}{3}\right)\tilde{\tau}^{3/2}\tilde{\rho}^{-1/2}\tfrac{1}{|\beta\Delta\mu|^{1/2}}(\gamma_4\omega)^{1/2}\mathcal{L} + \\ &\tfrac{18}{5}\left(\tfrac{4\pi}{3}\right)\tilde{\tau}^2\tilde{\rho}^{-1}\tfrac{1}{|\beta\Delta\mu|}\mathcal{L} + \\ &\tfrac{6}{5}\left(\tfrac{4\pi}{3}\right)\tilde{\tau}(\gamma_4\omega)\mathcal{L},\end{aligned} \tag{2.20}$$

5. bipolar spherical droplets, $\omega \ll 1, \omega \ll v^{1/3}$

$$\begin{aligned}&\beta\Delta G_* \cong 4\left(\tfrac{4\pi}{3}\right)\tilde{\tau}^3\tilde{\rho}^{-2}\tfrac{1}{|\beta\Delta\mu|^2} + \tfrac{6}{5}(\gamma_4\omega)\left(\tfrac{4\pi}{3}\right)\tilde{\tau}^2\tilde{\rho}^{-1}\tfrac{1}{|\beta\Delta\mu|} + \\ &\tfrac{12}{25}\left(\tfrac{4\pi}{3}\right)\tilde{\tau}^2\tilde{\rho}^{-1}\tfrac{1}{|\beta\Delta\mu|}\mathcal{L}\end{aligned} \tag{2.21}$$

In the next chapter, we plot these barriers for rod-like particles and semi-flexible worms.We investigate the importance for the Laplace-pressure contribution versus quench depth. The critical droplet volume scales as $\tau^3/|\beta\Delta\mu|^3$ so for large quench depth, the droplet volume will diminish. We expect to see an increase in Laplace pressure contribution as Laplace pressure becomes increasingly important for droplets with diminishing size.

| droplet type | critical droplet volume $v_*$ |
|---|---|
| homogeneous spherical | $\left(\frac{4\pi}{3}\right)\omega_3^3\tilde{\tau}^3\tilde{\rho}^{-3}\frac{1}{\lvert\beta\Delta\mu\rvert^3}(1+\sqrt{1+\frac{2}{5}\mathcal{L}\frac{\tilde{\rho}\lvert\beta\Delta\mu\rvert}{\tilde{\tau}}})^3$ |
| bipolar spherical | $\left(\frac{4\pi}{3}\right)\tilde{\tau}^3\tilde{\rho}^{-3}\frac{1}{\lvert\beta\Delta\mu\rvert^3}(1+\sqrt{1+\frac{2}{5}\tilde{\mathcal{L}}\frac{\tilde{\rho}\lvert\beta\Delta\mu\rvert}{\tilde{\tau}}})^3$ |
| homogeneous elongated | $8\left(\frac{4\pi}{3}\right)\omega_1^3\tilde{\tau}^3\tilde{\rho}^{-3}\frac{1}{\lvert\beta\Delta\mu\rvert^3}(1+\sqrt{1+\frac{6}{25}\mathcal{L}\frac{\tilde{\rho}\lvert\beta\Delta\mu\rvert}{\tilde{\tau}}})^3$ |
| bipolar elongated | $\pi\left(\frac{15}{8}\right)^{3/2}\omega_2^{5/2}\tilde{\tau}^{5/2}\tilde{\rho}^{-5/2}\frac{1}{\lvert\beta\Delta\mu\rvert^3}(1+\sqrt{1+\frac{2}{3}\mathcal{L}\frac{\tilde{\rho}\lvert\beta\Delta\mu\rvert}{\tilde{\tau}}})^{5/2}$ |

Table 2.3: critical droplet volumes for a solution containing semi-flexible worms

## 2.5 Conclusions

The barrier height depends on the volume $V$, the anchoring strength $\omega$, the surface tension $\tau$, the elastic constants $K_{11}$ and $K_{33}$ and the Laplace pressure. As the quench depth is increased, we expect the Laplace pressure to become more important as the droplet volume decreases. This we can deduce from the fact that the droplet volume is inversely proportional to the quench depth and the fact that this increases the droplet curvature (and thus Laplace pressure). This we investigate in the next chapter.

# Chapter 3

# Nucleation barriers for hard rods and semi-flexible worms

## 3.1 Introduction

In this chapter we calculate the nucleation barriers for the formation of a nematic phase in dispersions of both hard rods and of semi-flexible worms. In the previous chapter we found the qualitative barriers for the various droplet regimes in terms of the scaled, dimensionless parameters for the density, the surface tension, the extrapolation length and the Laplace pressure. Different free energies and scaling arguments describe these parameters depending on whether the particles are rigid, rod-like molecules or semi-flexible worms. We investigate both free energies and the scaling relations of these parameters and subsequently explicitly calculate the barriers for both particle types. We find that the Laplace pressure contribution cannot be neglected for small critical nuclei, which form following a deep quench. With increasing quench depth we see after reaching a certain concentration, that the limit of validity of classical nucleation theory will be reached as the droplet size approaches the size of the constituent particles. We explore this limit and in a following chapter, we use a different approach to calculate the free energies of the critical nuclei.

## 3.2 Free energy and scaling theory of rod-like particles

We begin this section with a brief introduction to the virial theory of the isotropic-nematic transition for hard rods (hard interactions between two rods are those that exhibit excluded volume interaction, meaning that the rods cannot interpenetrate each other) as described by Onsager [16]. In the 1940s Onsager treated the isotropic-nematic transition with a virial expansion of the free energy. For slender hard particles, the transition occurs at very low volume fraction and the virial expansion may be truncated after the second virial term leading to an exact theory for infinitely slender particles. From the expression for the free energy we derive a measure for the quench depth, $\beta\Delta\mu$. The barriers depend on a number of parameters, such as anisotropic surface tension, density, extrapolation length and Laplace pressure, in order to calculate the barriers explicitly we investigate their scaling relations.

The virial expansion of the Helmholtz free energy of the solute $\Delta F$ is given by [7]

$$\frac{\Delta F}{Nk_BT} = \ln(\rho) - 1 + \int f(\mathbf{u}) \ln[4\pi f(\mathbf{u})] d^2\mathbf{u} - \frac{1}{2}\int\int \beta_1(\mathbf{u},\mathbf{u}') f(\mathbf{u}) f(\mathbf{u}') d^2\mathbf{u} d^2\mathbf{u}', \qquad (3.1)$$

where $\Lambda$ is the thermal wavelength, $\beta_1$ equals the excluded volume between two particles inclined at $\mathbf{u}$ and $\mathbf{u}'$ and $f(\mathbf{u})$ is a non-uniform orientation distribution function, which gives the probability of finding a particle with an orientation characterised by the solid angle $d^2\mathbf{u}$. This distribution function is normalised

$$\int f(\mathbf{u}) d^2\mathbf{u} = 1 \qquad (3.2)$$

In the isotropic phase, all orientations are equally probable which implies $f_{iso}(\mathbf{u}) = 1/4\pi$. In the nematic phase, the orientation is governed by the first integral in eq. (3.1). The second integral in this equation equals the second virial coefficient and corresponds to interactions between the two particles.

For long hard rods of diameter $D$ and length $L$, the parameter $-\beta_1$ equals the volume excluded to a second rod due to the presence of the first rod and is dependent on the angle $\gamma$ between them and is for end-capped cylinders given by [7]

$$-\beta_1 = 2L^2D|\sin\gamma| + 2\pi D^2 L + \frac{4}{3}\pi D^3 \qquad (3.3)$$

The last two terms are end corrections which are at least of order $D/L$ smaller than the leading term. The end corrections depend on the exact form of the rods near the ends and are, for example, different for simple, non end-capped cylinders. For thin rods these end effects are of minor importance, thus giving [24]

$$\beta_1 \sim -2L^2D|\sin\gamma| \tag{3.4}$$

An expression for the free energy of hard rods which describes the isotropic-nematic transition is found when eq. (3.4) is combined with eq. (3.1) and by introducing a dimensionless concentration $c$ [7]

$$c \equiv \frac{\pi}{4}L^2D\rho, \tag{3.5}$$

where $\rho$ is the density $N/V$, with $N$ the number of particles and $V$ the volume, and $b \equiv (\pi/4)L^2D$ is half the excluded volume between two rods if they are randomly oriented [24]. The free energy can now be expressed as [7]

$$\frac{\Delta F}{NkT} \approx constant + \ln c + \sigma(f) + c\varrho(f), \tag{3.6}$$

where $\sigma(f)$ is related to the orientational entropy as given by the first integral in eq. (3.1). For the isotropic phase, $\sigma = 0$. $\varrho$ can be seen as the packing entropy [7]

$$\varrho(f) \equiv \frac{4}{\pi}\int\int |\sin\gamma| f(\mathbf{u})f(\mathbf{u}')d^2\mathbf{u}d^2\mathbf{u}' \tag{3.7}$$

For the isotropic phase, $\varrho = 1$. For low particle concentrations the orientational entropy dominates and an isotropic phase is favoured, whereas for high concentration the packing entropy dominates and a nematic phase is favoured. It is the competition between these two which drives the isotropic-nematic transition.

The free energy has a minimum for a given concentration $c$. By choosing a trial function with one or more variational parameters, then calculating the free energy as a function of these parameters and next minimising it with respect to these parameters this minimimum can be

found. In chapter five we investigate the possibility of doing so, choosing the normalised Onsager trial function.

From the expression of the free energy the chemical potential $\mu$ of hard rods can be calculated using the thermodynamic relation $\mu = (\partial \Delta F / \partial N)_{V,T}$ leading to [24]

$$\beta\mu = const. + \ln\rho + \sigma + 2c\varrho \tag{3.8}$$

In the isotropic phase, the expression for $\mu$ becomes

$$\beta\mu = const + \ln\rho + 2c \tag{3.9}$$

For each concentration $c$ the system of hard rods must be at the minimum of the free energy. Above a certain concentration this minimum is obtained by a state in which part of the system is isotropic and the other part is nematic with different concentrations for the isotropic $c_i = 3.29$ and the nematic $c_{nem} = 4.19$. [24]. We can now calculate the quench depth $\Delta c = c - c_i$. The concentration quench is therefore the increase of the concentration of particles in the coexisting phase. We find this expression by calculating the chemical potential difference of the critical nucleus and the isotropic bulk phase (of which the chemical potential equals the new phase were it a bulk nematic)

$$\beta\Delta\mu = \ln(\frac{c_i}{b}) + 2c_i - \ln(\frac{c_i + \Delta c}{b}) - 2(c_i + \Delta c) \tag{3.10}$$

In this expression we used $c_i = b\rho$ where $b = (\pi/4)L^2D$. After some algebraic manipulation and a Taylor expansion to the first order with respect to $\Delta c/c_i$ we find

$$\beta\Delta\mu = (\frac{1}{c_i} + 2)\Delta c + ... \tag{3.11}$$

Now we can deduce the following relation between chemical potential difference and quench depth, $\beta\Delta\mu \approx 2.30\Delta c$.

The osmotic pressure is calculated rom the expression for the free energy 3.6, the thermodynamic relation $p = -(\partial \Delta F / \partial V)$ and the Gaussian distribution function [24]

$$p = 3\rho kT \tag{3.12}$$

In order to calculate the barriers for rigid rods, we use scaling relations found in literature for the surface tension $\tau$, the droplet density $\rho$, the pressure $p$ and elastic constant $K_{11}$ and make them dimensionless by scaling them to the extrapolation length $\xi$ see table 3.1.

| **quantity** | $\xi$ | $\mathcal{L}$ | $\tilde{\tau}$ | $\tilde{\rho}$ |
|---|---|---|---|---|
| definition | $K_{11}/\tau\omega$ | $\tau(p\xi)^{-1}$ | $\beta\xi^2\tau$ | $\xi^3\rho$ |
| hard rod result | $(7/8)(c/\pi)L\omega^{-1}$ | $2/21(\pi/c)^2\omega$ | $7/8(c/\pi)^2\omega^{-2}L/D$ | $4(7/8)^3(c/\pi)^4\omega^{-3}L/D$ |

Table 3.1: The dimensionless parameters are given in the first row, the second row contains their definition and in the third row these are given in terms of the nematic concentration, the anchoring strength $\omega$ and the aspect ration of the, presumedly hard rod, particles $L/D$

Here we have used $\tau = k_BT/LD$ [25], $\rho = 4c/\pi L^2D$ [7], $K_{22}D/k_BT = (7/96)L^2D\rho$ [26] [27], $K_{11} = 3K_{22}$, $p = 3\rho kT$ [27] and $c$ is taken to be $c_{nem} = 4.19$ [24] as the given relations are for the nematic phase.

## 3.3 Free energy and scaling theory of semi-flexible worms

In Onsager's theory, the system described consisted of long thin hard rods such as TMV. For particles which exhibit some degree of flexibility, such as PBG, the theory has to be modified. PBG can be described as what is called a semi-flexible worm, which is locally very stiff but is long enough to form coils in a dilute solution. This can be expressed as contourlength $L \gg$ persistence length $P \gg$ diameter $D$. The contourlength is the actual length of the coils stretched out. The persistence length is the characteristic length scale on which the direction vector $\mathbf{u}$ of the chain changes direction due to thermal agitation, see figure (3.1). It is the flexibility of the worms with which is associated a configurational entropy. In the nematic phase, all particles more or less align in parallel with the director, which leads to a loss in configurational entropy. This entropy replaces the orientational entropy for rods in eq. (3.1). [7]

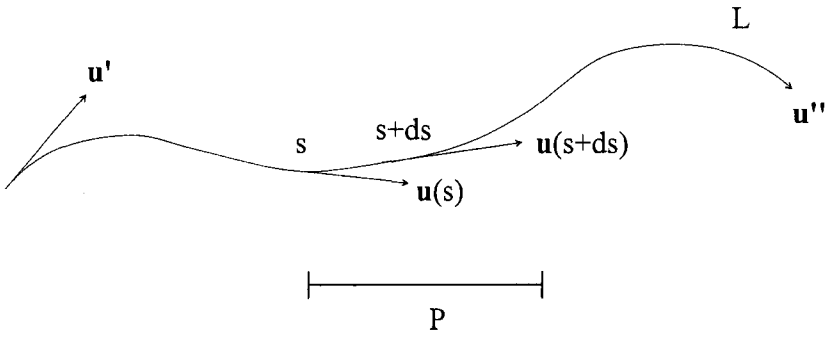


Figure 3.1: a typical configuration of a semi-flexible worm of length L and persistence length P; s measures the distance along the contour of the chain and $\mathbf{u}(s)$ is the tangent to the chain at this point.

We consider a solution of volume $V$ containing $N$ rods and length $L$ and diameter $D$. When we now divide each rod in to $L/l$ (sub)rods of length $l$, the number of rods increases but their length decreases by the same factor, keeping the combination $NL$ constant. Therefore, this system has approximately the same second virial term as the system for hard rods as described by Onsager. The second virial term is build up from independent, local, rod-like two-particle interactions. Because on a length scale $l$ ($P >> l >> D$) a semi-flexible worm is rod-like, two semi-flexible worms locally interact like rods. [7] This means that it is possible to describe half the excluded volume $b_p$ when $P >> D$ between two worms as [24]

$$b_p = \frac{\pi}{4}(\frac{L}{P})^2 P^2 D = \frac{\pi}{4} L^2 D = (\frac{L}{P})^2 b_m, \tag{3.13}$$

where half the excluded volume $b_p$ is rescaled to $b_m$, a quantity related to the persistence segments $L/P$. This approximation treats each worm-like chain as if it were a collection of rigid $L/P$ persistence length fragments. This means that eq.3.6 can be used as the expression for the free energy of worm-like particles, and can now be written as [24]

$$\frac{\Delta F}{N k_B T} \approx constant + \ln \rho_p + \sigma_p(f) + c\varrho_p(f) \tag{3.14}$$

Rescaling the polymer chain variables $\rho_p$ and $b_p$ to quantities related to persistence segments $\rho_p \equiv (P/L)\rho_m$ and $b_p \equiv (L/P)^2 b_m$ and since the orientational free energy is also extensive,

$\sigma \equiv (L/P)\sigma_m$, eq. (3.14) can then be written as [24]

$$\frac{\Delta F}{NkT} \approx constant + \ln \frac{P}{L}\rho_m + \frac{L}{P}\sigma_m(f) + \frac{L}{P}c\varrho_m(f) \tag{3.15}$$

As $L >> P$, we can ignore the logarithmic term and as for the isotropic phase $\sigma = 0$ and $\varrho = 1$, we can write the free energy as

$$\frac{\Delta F}{NkT} \approx \frac{L}{P}c \tag{3.16}$$

We proceed as for hard worms, using the thermodynamic relation $\mu = (\partial \Delta F/\partial N)_{V,T}$ and the free energy of 3.1 the difference in chemical potential $\beta\Delta\mu$ can be expressed as the quench depth

$$\beta\Delta\mu \approx 2\Delta c\frac{L}{P} \tag{3.17}$$

The concentration where the isotropic phase is at equilibrium is at $c_i = 5.41$ and the concentration where the nematic phase is at equilibrium is at $c_{nem} = 6.20$, see [24]. We now continue our scaling analysis by examining the scaling relations of other dimensionless parameters determining the free energy of the droplet, see table 3.2. Here we have used $\tau = 0.442k_BT/PD$ [28], $\rho = 4c/\pi P^2 D$ [7], the osmotic pressure is as in eq. 2.15, $K_{22}D/k_BT = (7/96)P^2D\rho$ [26] [29], $K_{11} = 3K_{22}$ [27] and $c$ is taken to be the nematic concentration as the relations apply to the nematic so $c_{nem} = 6.197$. [24]

| **quantity** | $\xi$ | $\mathcal{L}$ | $\tilde{\tau}$ | $\tilde{\rho}$ |
|---|---|---|---|---|
| definition | $K_{11}/\tau\omega$ | $\tau(p\xi)^{-1}$ | $\beta\xi^2\tau$ | $\xi^3\rho$ |
| hard worm result | $0.7(c/\pi)P\omega^{-1}$ | $0.182c^{-8/3}\omega$ | $0.216(c/\pi)^2\omega^{-2}P/D$ | $1.372(c/\pi)^4\omega^{-3}P/D$ |

Table 3.2: The dimensionless parameters are given in the first row, the second row contains their scaling relations and in the third row these scaling relations are given in terms of the nematic concentration, the anchoring strenght $\omega$ and the aspect ration of the particles $P/D$

With scaling relations for both hard rods and semi-flexible worms we can now calculate nucleation barriers for solutions containing these particles.

## 3.4 Nucleation barriers

The barrier height for a solution containing rigid rods is shown as a function of the quench depth in figures (3.2) and (3.3). As the barrier height is proportional to $L/D(\Delta c)^{-2}$ for droplets for both small and large $\omega$ this factor is trivial and is therefore removed by multiplying the barrier height with $D/L(\Delta c)^2$. By doing so we can focus on the changes of the behaviour of the barrier for increased quench depth. The most striking feature is the increasing importance of the Laplace pressure for increasing quench depth, this is consistent with the fact that for an increase in quench depth the droplets decrease in size. In figure (3.2), where $\omega = 0.1$ the transition from a bipolar spherical droplet to a homogeneous spherical droplet without Laplace contribution occurs at $\Delta c = 0.37$, the transition from a bipolar spherical to a homogeneous spherical droplet with Laplace pressure at $\Delta c = 0.53$. From this we can see that the Laplace pressure shifts the quench depth towards the spinodal for which the transition occurs. The transition with and without Laplace pressure occurs before the spinodal at $\Delta c = 0.70$ is reached. In figure (3.3), where $\omega = 10$, we see a different picture, the first transition without Laplace pressure contribution is a bipolar elongated droplet transforming into a homogeneous elongated droplet and occurs at $\Delta c = 0.05$. The next transition is a bipolar spherical transforming into a homogeneous elongated droplet and occurs at $\Delta c = 1.07$. When the Laplace pressure is included, the only transition occurs at $\Delta c = 0.08$ and is from a bipolar spherical droplet to a homogeneous elongated droplet. Again, we see a shift of the droplet transition toward the spinodal. The latter two transitions described are not likely to occur.

The barrier height for a solution containing semi-flexible worms, is shown as a function of the quench depth is in figures (3.4), (3.5). Similar to the barrier height of the rod-like particles the barrier height is proportional to $P/D(\Delta c)^-2$ for droplets for both small and large $\omega$, this factor is trivial and is therefore removed by multiplying the barrier height with $D/P(\Delta c)^2$. In these cases, the quench depth is found to scale as $P/L$ (see eq. 3.17) and is therefore removed from the curves by multiplying the quench depth with $L/P$. A significant difference from the rods is the fact that the Laplace pressure contribution has far less impact on worms. In figure (3.4),

where $\omega = 0.1$, the transition without Laplace pressure contribution from a bipolar droplet to a homogeneous one is at $\Delta c = 0.66$ and with Laplace pressure this is at $\Delta c = 0.46$. We see that the Laplace pressure causes a shift away from the spinodal at $\Delta c = 0.6$. In figure (3.5), where $\omega = 10$, we see that the first transition from a bipolar elongated to a homogeneous elongated droplet occurs at $\Delta c = 0.004$, a second transition from a bipolar spherical to a homogeneous elongated droplet occurs at $\Delta c = 0.01$, a third transition from a bipolar spherical droplet to a bipolar elongated droplet occurs at $\Delta c = 0.02$. In this figure it becomes evident that the influence of the Laplace pressure contribution to the quench depth is minimal, as the distinction between the curves with and without Laplace pressure contribution can no longer be discerned at the transitions.

We see in the figures (3.2), (3.3), (3.4) and (3.5) for both rods and worms and $\omega = 0.1$ and $\omega = 10$ that both the bipolar droplets are lower in energy than the the homogeneous droplets for shallow quenches, this is explained by the fact that the energy costs for bipolar droplets is lower, as it goes like $\tau^3/(\Delta c)^2$, than for homogeneous droplets for which the barrier height scales as $(\tau + O(\omega))^3/(\Delta c)^2$.

| | |
|---|---|
| *he* | homogeneous elongated |
| *be* | bipolar elongated |
| *hs* | homogeneous spherical |
| *bs* | bipolar spherical |

Table 3.3: abbreviations used in figures (3.2), (3.3), (3.5), (3.4), (3.6) and (3.7).

We must remark that the transitions between the droplet types are continuous in contrast to what is depicted here. The free energies used to calculate the barriers are asymptotic limits, meaning that they represent extreme droplet types. This is why the transitions from a homogeneous droplet to a bipolar droplet as shown in figures (3.2), (3.3), (3.5) and (3.4) are not continuous. In order to depict the actual continuous transition, interpolation functions for the crossover between the homogeneous and the bipolar droplet types need to be calculated for both

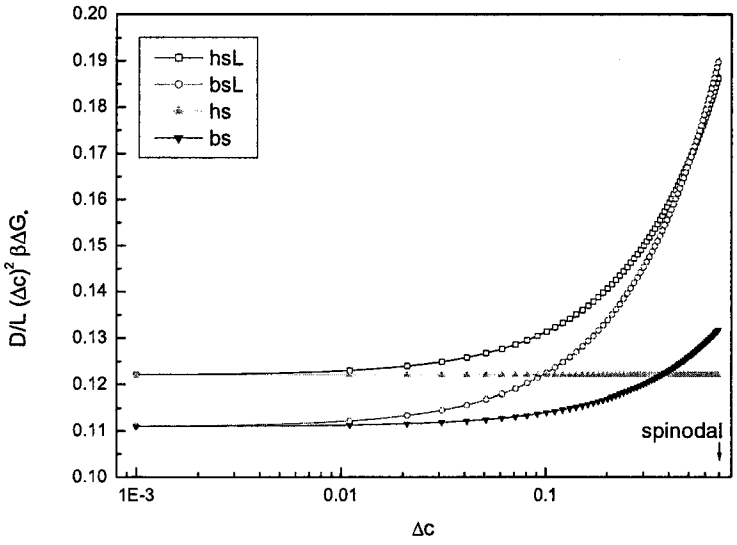


Figure 3.2: Dimensionless nucleation barrier of a solution containing hard rods for small $\omega$, L denotes that the Laplace pressure is included. Points in this graph are used to show which droplet type belongs to which line.

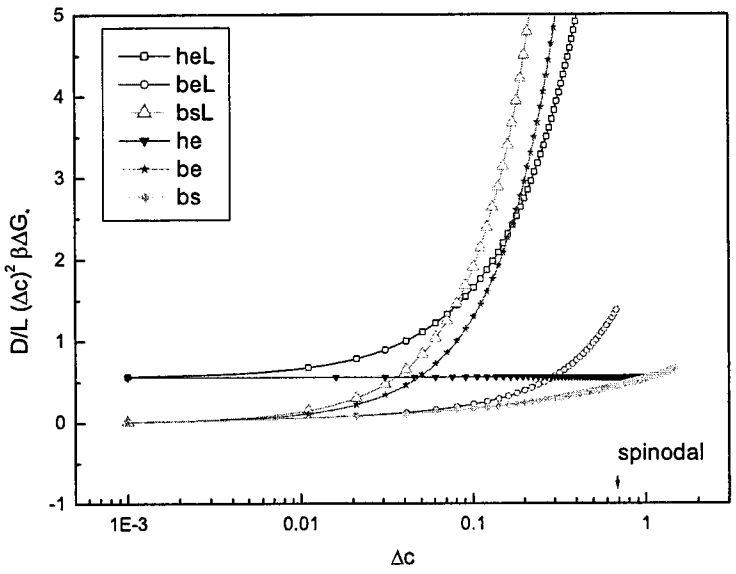


Figure 3.3: Dimensionless nucleation barrier of a solution containing hard rods for $\omega = 10$, L denotes that the Laplace pressure is included.

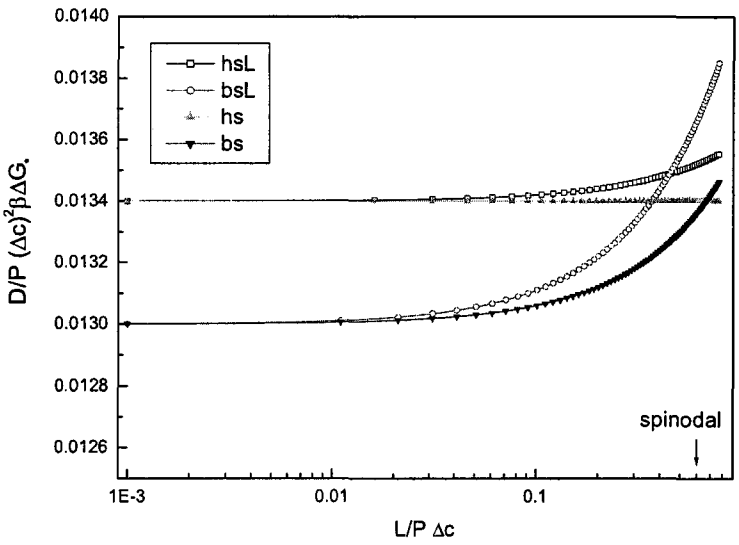


Figure 3.4: Dimensionless nucleation barrier of a solution containing semi-flexible worms for $\omega = 0.1$, L denotes that the Laplace pressure is included.

$\omega \ll 1$ and $\omega \gg 1$.

## 3.5 CNT limit

As the quench depth is increased, the critical critical droplet size decreases, approaching the limit where droplet size equals particle size. For all droplet types, except the bipolar spherical droplet (where $V_*/L = 1$ for $\Delta c = 0.77$), we see from figures (3.6) and (3.7) this limit is reached before the spinodal. At this point the internal structure of the droplet will have to be considered when calculating the free energy of the droplet. For future work we explore the possibility in chapter 5 regarding density functional theory for the nematic droplets.

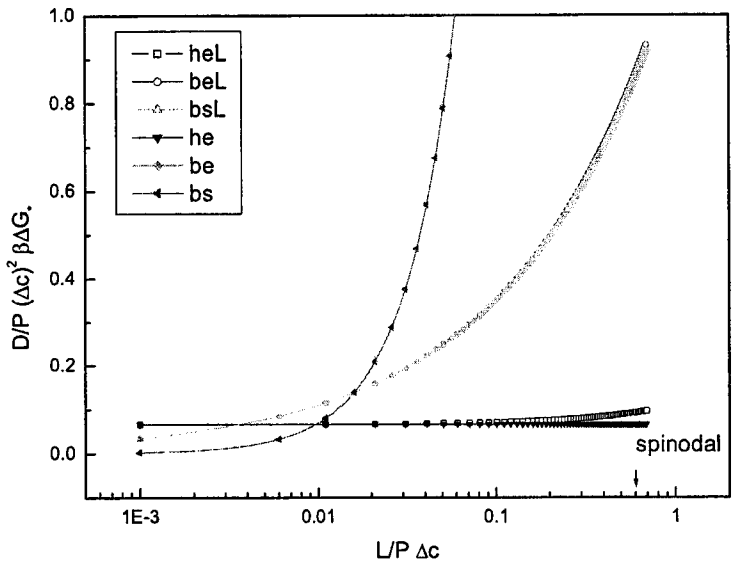


Figure 3.5: Dimensionless nucleation barrier of a solution containing semi-flexible worms for $\omega = 10$, L denotes that the Laplace pressure is included.

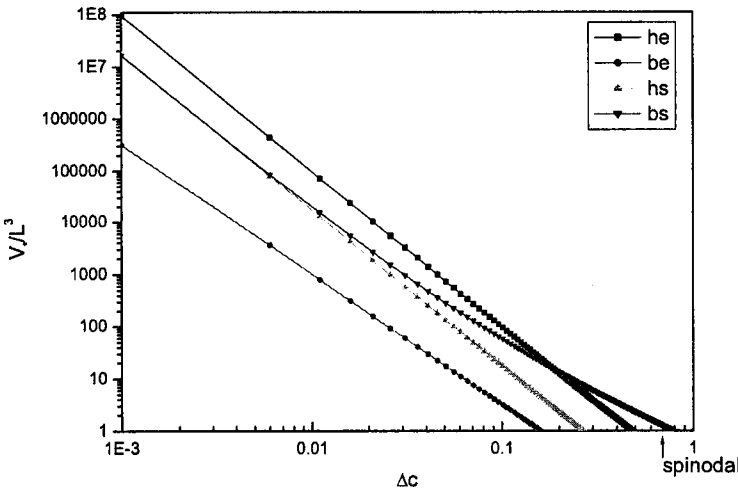


Figure 3.6: Droplet containing rod-like particles. When $V_*/L^3$ equals 1, the critical droplet has become of the same size of the particle.

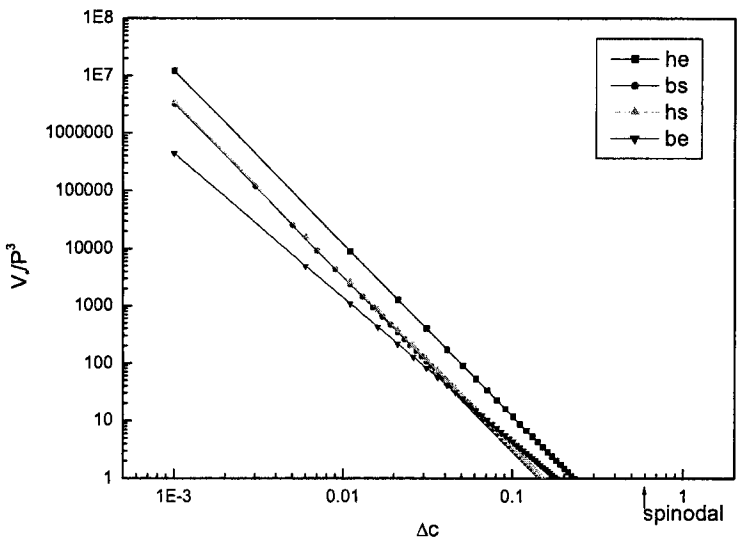


Figure 3.7: Droplet containing semi-flexible worms. When $V_*/P^3$ equals 1, the critical droplet has become of the same size of the particle.

## 3.6 Conclusions and discussion

We have seen for a solution containing hard rods that for deep quenches, which results in small droplets, the Laplace pressure becomes important. The transitions between the droplet types are shifted toward the spinodal.

A solution containing worms exhibit a different behaviour. The Laplace pressure contribution is of much less importance, this is could be caused by the fact that the semi-flexible worms have less resistance to the curvature of the droplet than the rigid rod-like particles. The transitions are shifted away from the spinodal.

The transitions between the droplet types at $\omega = 10$ are expected to start with bipolar spherical, then bipolar elongated and then finally, homogeneous elongated [6]. This is not in agreement with figures (3.3) and (3.5). This is is most likely a computational error.

The limit of Classical Nucleation Theory (CNT) is reached before the spinodal, so the neces-

sity arises to find an expression for the free energy of the droplet by describing the Helmholtz free energy as a functional of the nonuniform generalized density distribution. Another important matter is the CNT breakdown at quench depths near the spinodal, although Laplace pressure is found to be significant at high quench depth, it is no longer relevant after CNT is no longer valid.

Now that we have calculated the nucleation barriers for hard rod-like particles, it is possible to calculate the nucleation rate discussed in the following chapter.

# Chapter 4

# Nucleation Kinetics

## 4.1 Introduction

In this chapter we present results of the calculation of the nucleation rates of the hard rod nematic of the five scaling regimes we have described earlier. We investigated the nucleation rate of hard rods only, because the theory for semi-flexible worms is not as well developed. [5] Experiments have shown a pronounced maximum of the nucleation rate, [2] which has not been explained theoretically to date.

As mentioned in Chapter 1, the nucleation rate is given by as the thermodynamic probability of having a fluctuation leading to a critical nucleus times a dynamical factor $\mathcal{A}$ describing the rate at which the nucleus grows [12]

$$I_s = \mathcal{A} \exp[-\beta \Delta G_*], \tag{4.1}$$

where $\beta \Delta G_*$ is the height of the nucleation barrier, which is the minimum amount of reversible work expended for the formation of a nucleus. Which we calculated in the previous chapter. Near the spinodal the nucleation barrier becomes small (in fact, the barrier should disapear altogether at the spinodal), and therefore, the dynamical prefactor begins to dominate.

We first examine the general theoretical ingredients of the kinetic prefactor as previously

described for the crystallisation of liquids [12] [30] [11] [14]. We then apply a recent kinetic theory [5] describing the kinetics of hard rods at the initial phase of spinodal decomposition, to calculate the prefactor of the nucleation rate. This theory assumes the process that drives the mass transport to be collective diffusion, as opposed to self diffusion. It enables us to explain the maximum found in the experiments as the critical slowing down of the nucleation dynamics of the nematic phase near the spinodal.

## 4.2 The kinetic prefactor

Let us first consider the kinetic theory that describes the rate and mechanism by which nematic droplets grow or shrink by gaining or losing particles. The equilibrium number of nuclei can be described as [31]

$$N_n^e = N^i \exp[-\beta \Delta G_n], \tag{4.2}$$

where $N^i$ the number of particles in the isotropic phase. As mentioned in the previous chapter, the free energy goes through a maximum, the nucleus size corresponding to this maximum is called the critical nucleus size $n^*$. Nuclei smaller than the critical nucleus size tend to shrink by losing particles, whilst nuclei larger than the critical nucleus size tend to grow by gaining particles.

In order to describe nucleation dynamics with rate equations a number of assumptions need to be made: 1) The whole process is in local thermal equilibrium; 2) There is no correlation between successive events that change the particle number in a nucleus, i.e., the nucleus has no memory; 3) It is indeed possible to assign a particle number to the nucleus; 4) Nuclei grow or shrink by gaining or losing single particles. [30] This last assumption can be described as [11]

$$E_{n-1} + E_1 \underset{k_n^-}{\overset{k_{n-1}^+}{\rightleftharpoons}} E_n \tag{4.3}$$

$$E_n + E_1 \underset{k_{n+1}^-}{\overset{k_n^+}{\rightleftharpoons}} E_{n+1}, \tag{4.4}$$

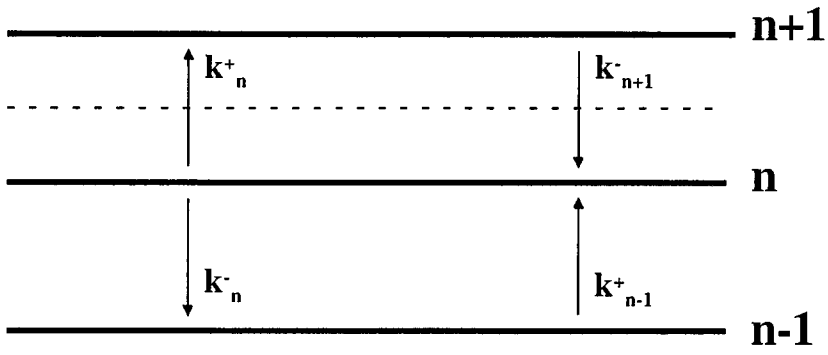


Figure 4.1: forward and backward rates, the flux goes though the dotted line

where $E_n$ represents a nucleus of $n$ particles and $E_1$ a single particle, $k_n^+$ is the rate of particle addition (the forward rate constant), which depends on the concentration of single particles in the surrounding medium, and $k_n^-$ is the rate of particle loss (the backward rate constant) to a nucleus of size $n$. This equation expresses the actual kinetic mechanism of nucleus formation. This leads to the time-dependent nucleus density $N_{n,t}$, consisting of coupled rate equations for the nucleus densities $N_{n,t}$ of nuclei of size $n$ at time $t$ [12]

$$\frac{d}{dt}N_{n,t} = N_{n-1,t}k_{n-1,t}^+ - [N_{n,t}k_n^- + N_{n,t}k_n^+] + N_{n+1,t}k_{n+1}^-, \tag{4.5}$$

The nucleation rate at a nucleus size $n$ is the time-dependent flux of nuclei past that size, in other words, the net rate at which nuclei of size $n$ become nuclei of size $n+1$, see figure 4.1.

$$I_{n,t} = N_{n,t}k_n^+ - N_{n+1,t}k_{n+1}^- \tag{4.6}$$

In a steady state, the nucleus density of nucleus with $n$ particles, $N_n^s$,does not depend on time . [12]

$$I_s = N_n^s k_n^+ - N_{n+1}^s k_{n+1}^- \tag{4.7}$$

The nucleation rate is zero when the initial phase is in thermal equilibrium so eq. (4.7) with nucleus density of nucleus with $n$ particles in equilibrium $N_n^e$, then gives

$$N_n^e k_n^+ = N_{n+1}^e k_{n+1}^- \tag{4.8}$$

Using this expression to determine $k_{n+1}^-$, the steady-state nucleation rate can be written as [12]

$$I_s = N_n^e k_n^+ \left[\frac{N_n^s}{N_n^e} - \frac{N_{n+1}^s}{N_{n+1}^e}\right] \tag{4.9}$$

It can be assumed that as $n \to 0$, $N_n^s \to N_n^e$ and that as $n \to \infty$, $N_n^s \to 0$. These boundary conditions are more conveniently written as

$$\left.\begin{array}{ll} n \leq u, & N_n^s = N_n^e \\ n \geq v, & N_n^s = 0 \end{array}\right\}, \tag{4.10}$$

where $u < n^* < v$. Fortunately, the final result is not strongly dependent on the values chosen for u and v, provided they are outside the critical region. Summing eq. 4.9 for all values of $n$ between $u$ and $v$ and using the stated boundary conditions leads to [31]

$$I_s \sum_u^v \frac{1}{N_n^e k_n^+} = \frac{N_u^s}{N_u^e} - \frac{N_{v+1}^s}{N_{v+1}^e} = 1 \tag{4.11}$$

So, the expression for the steady state nucleation rate in terms of forward rate constants becomes

$$I_s = \left[\sum_u^v \frac{1}{N_n^e k_n^+}\right]^{-1} \tag{4.12}$$

$I_s$ is obtained by evaluating the sum for $n$ near $n^*$, making several assumptions. 1) The terms for the sum for values $n$ near $n^*$ dominate since $\Delta G_n$ has a maximum at $n^*$; 2) $k_n^+ \to k_{n^*}^+$; 3) $N^i$ is taken to be equal to the total number of particles in the system; 4) Replace $\Delta G_n$ by the first two nonzero terms in a Taylor expansion about $n^*$, so that $\exp[-\beta\Delta G]$ can be written as [30]

$$\exp[-\beta\Delta G] = \exp[-\beta\Delta G(n^*)] \exp[\frac{1}{2}\beta|\Delta G''(n^*)|(n-n^*)], \tag{4.13}$$

where $\Delta G''(n^*) = \partial^2 \Delta G/\partial n^2$; 5) If the critical nucleus $n^*$ is large enough, then many terms near $n^*$ contribute to the sum and it can be replaced by an integral from $n - n^* = -\infty$ to $n - n^* = \infty$, taking $N_n^e$ to be a continuous function of $n$.

The expression for the nucleation rate $I_s$ becomes

$$I_s = N^i k_{n^*}^+ \exp[-\beta\Delta G(n^*)] \left[\int_{-\infty}^{\infty} \exp[-\frac{1}{2}|\beta\Delta G''|(n-n^*)^2] dn\right]^{-1} \tag{4.14}$$

Which after evaluation of the integral, gives

$$I_s = N^i k_{n^*}^+ \sqrt{\frac{\beta|\Delta G''(n^*)|}{2\pi}} \exp[-\beta \Delta G(n^*)], \tag{4.15}$$

with $\sqrt{\beta|\Delta G''(n^*)|/2\pi}$ the so-called Zeldovich factor. This factor signifies the fact that not all particles at the top of the nucleation barrier end up in the nematic phase, but can also recross and end up in the isotropic phase [13].

The next problem in formulating the nucleation kinetics is to derive expressions for the rate constants $k_n^+$. In a condensed system it is possible to define an average, unbiased particle jump frequency $\gamma$ at the nucleus surface. If a particle jumps from one phase to the other there will be a free energy change. Suppose that the free energy of a nucleus $E_{n+1}$ exceeds that of $E_n$ by $\Delta g_n$. According to reaction rate theory, [32] the probability of the activated state to occur and the jump frequency at the droplet interface (taking the particle from one local configuration to a new one)

$$\gamma_n^+ = \gamma \exp[-\Delta g_n / 2kT], \tag{4.16}$$

where $\gamma_n^+$ is the average jump rate of particles in the forward and backward reactions of eq. 4.4. The rate constant $k_n^+$ is proportional to $O_n$, the number of sites where the transformation from one phase to the other is possible. It is assumed that $O_n$ is the number of particles that could be placed with their centers on a sphere that just encloses all the particles in the nucleus. It is possible to use a sphere-approximation when the relevant length scale is taken as the length of the tactoid. In that case it does not matter whether the nucleus is spherical or elongated. The number of sites is the surface area of the sphere bounding the nucleus divided by an area per particle (taken to be $\pi r^2$, where $r$ is the radius of a sphere of the particle volume). We then obtain [12]

$$O_n = 4n^{2/3}. \tag{4.17}$$

We write the forward rate constant $k_n^+$ as $k_n^+ = O_n \gamma_n^+$, resulting in

$$k_n^+ = 4n^{2/3} \gamma \exp[-\frac{1}{2}\beta \Delta g_n], \tag{4.18}$$

with $\gamma$ being the jump frequency for diffusion

$$\gamma = \frac{6D}{\ell^2}, \tag{4.19}$$

with $\ell$ the particle jump distance and $D$ the relevant diffusivity. For $k_n^+ \to k_{n_*}^+$, $\Delta g_n$ can be ignored so the final expression for the forward rate constant becomes

$$k_{n_*}^+ \approx 4n^{2/3}\frac{6D}{\ell^2}. \tag{4.20}$$

The question is what the distance $\ell$ represents in an isotropic fluid containing nematic droplets. We assume this to be the linear scale of the tactoid itself. Because many particles are at a large distance from the nucleus, the only length scale the system available is the tactoid length. Inserting eq. (4.19) into eq. (4.18) and neglecting the exponential function (as the exponential term in eq. (4.15) is much larger) and inserting the result into eq. (4.15) leads to the nucleation rate per particle

$$I_s = \frac{24Dn^{2/3}N^i}{\ell^2}\sqrt{\frac{|\beta\Delta G_*''|}{2\pi}}\exp[-\beta\Delta G_*] \tag{4.21}$$

What is left is to determine the expression for the diffusion coefficient $D$. We do this by analysing the prevalent diffusion mechanism in the next section.

## 4.3 The diffusion coefficient

Ackerson and Schätzel [4] argue that crystal formation and growth are not governed by the particle self-diffusivity but the particle gradient diffusivity also known as collective diffusion. In their study of the crystallisation of hard sphere colloidal particles, they suggest that because of the crystal in the coexistence region is more dense than the metastable fluid or final fluid density, the crystal growth will produce a depletion region in the immediate vicinity of the crystal-liquid interface. As a result of this reduced particle density, particles will diffuse into this region from the metastable fluid. If the addition to the crystal results in a nonuniform crystal density, then the crystal will also relax to uniform density via diffusion. This diffusion should be governed by collective diffusion [4].

Winters, Odijk and Van der Schoot [5] described the collective diffusion mechanisms in a suspension of hard rods at the initial stage of spinodal decomposition with the and concluded that there are three modes, the self diffusivity mode, the pure orientation fluctuation mode and the pure density fluctuation mode. The density and orientation fluctuation modes can intermingle giving rise to hybrid modes with relaxation rates $\lambda_+$ or $\lambda_-$. The former is always stable so the driving force for phase transition needs to be found with the latter mode, which can become unstable at sufficiently high densities. The $\lambda_-$ mode is a coherent orientation translation mode. Particles with the same orientation remain unchanged, coherent, during transport. This results in a phase separation of groups containing particles with the same orientation that move by way of translational diffusion. The expression for this $\lambda_-$ mode is [5]:

$$\lambda_- = Dq^2(1 - \frac{c}{4} + \frac{11}{252}cq^2\frac{L^2}{4} + ...), \tag{4.22}$$

where $c$ is the particle concentration, $L$ defined earlier is the length of the particle and $q$ is the wavenumber. We set $q = (2\pi)/\ell$ with $\ell$ the length of the tactoid (see above). Because $(L/\ell)^2$ is negligible as $L \ll \ell$ only the first two terms of the right hand side of eq. (4.22) are considered relevant. The expression for the unstable mode $\lambda_-$ can be approximated as

$$\lambda_- = D(\frac{2\pi}{\lambda})^2(1 - \frac{c}{4} + ...) \tag{4.23}$$

This mode becomes unstable for $c > 4$, which is the concentration at which spinodal decomposition occurs. We use the diffusion coefficient of this expression to replace the diffusion coefficient $D$ in eq. (4.21), and exchanging $N^i$ with the density $\rho = N/V = c[(\pi/4)L^2D]^{-1}$ by multiplying 4.21 with volume $(\pi/4)L^2D$, we can write the final dimensionless expression for the nucleation rate $I_s$ as:

$$\tilde{I}_s = \frac{\pi}{4}\frac{L^4}{D_s^L}DI_s = 24(\frac{L}{D})^{2/3}(\frac{4}{\pi})^{2/3}c_{nem}^{5/3}(1 - \frac{c}{4})\sqrt{\frac{|\beta\Delta G_*|''}{2\pi}}\exp[-\beta\Delta G_{n^*}], \tag{4.24}$$

where $D_s^L$ is the long-time self diffusion coefficient, $c_{nem} = 4.2$ is the concentration at which a stable nematic phase is formed, and $L$ is the length and $D$ is the diameter of the rods. The concentration $c = 3.3 + \Delta c$, where $\Delta c$ represents the quench depth.

## 4.4 Results

We proceed by calculating the nucleation rates for the nematic droplets in five different scaling regimes. We find that the nucleation rates depend on the height of the nucleation barriers, the aspect ratio of the particles $L/D$, and the quench depth. The nucleation rates are given in table 4.1 and depicted in figure 4.4. The transitions between droplet types are not visible. All nucleation rates show a strong maximum, although this is not visible from 4.4, because the differences between the different droplet nucleation rates are very large as the differences between droplets are emphasized by the exponential function in the nucleation rate. In order to show the strong L/D dependence of the nucleation rates we show the nucleation rates for homogeneous elongated droplets. The choice for this droplet type is arbitrary. From figures 4.3 and 4.2 we can see that for increasing $L/D$ the nucleation rates strongly decrease. This is caused by the fact that the nucleation barrier, scaling as $L/D$, is the argument of the exponential function in eq. 4.24. Another important point we can see is the pronounced maximum observed in experiments and that at the spinodal, the nucleation rate rapidly decreases to zero. This slowing down is a phenomenon known as 'critical slowing down', which entails the slowing down of the dynamics of the fluctuations represented by the hybrid mode $\lambda_-$ in eq. 4.23.

| droplet types | dimensionless nucleation rate $\tilde{I}_s$ |
|---|---|
| homogeneous elongated | $191(L/D)^{1/6}(\Delta c)^2(1-c/4)(1+0.39\Delta c)\exp(-\beta\Delta G_*^{he})$ |
| bipolar elongated | $1090(L/D)^{1/6}(\Delta c)^{7/4}(1-c/4)(1+0.65\Delta c)\exp(-\beta\Delta G_*^{be})$ |
| homogeneous spherical | $318(L/D)^{1/6}(\Delta c)^2(1-c/4)(1+0.13\Delta c)\exp(-\beta\Delta G_*^{hs})$ |
| bipolar spherical ($\omega = 0.1$) | $139(L/D)^{1/6}(1-c/4)(46.2(\Delta c)^4+1590(\Delta c)^5)\exp(-\beta\Delta G_*^{bs})$ |
| bipolar spherical ($\omega = 10$) | $50.4(L/D)^{1/6}(1-c/4)(46.2(\Delta c)^4+796(\Delta c)^5-66.7(\Delta c)^7)\exp(-\beta\Delta G_*^{bs})$ |

Table 4.1: dimensionless nucleation rates for droplet types in five different regimes, where $c = 3.3 + \Delta c$

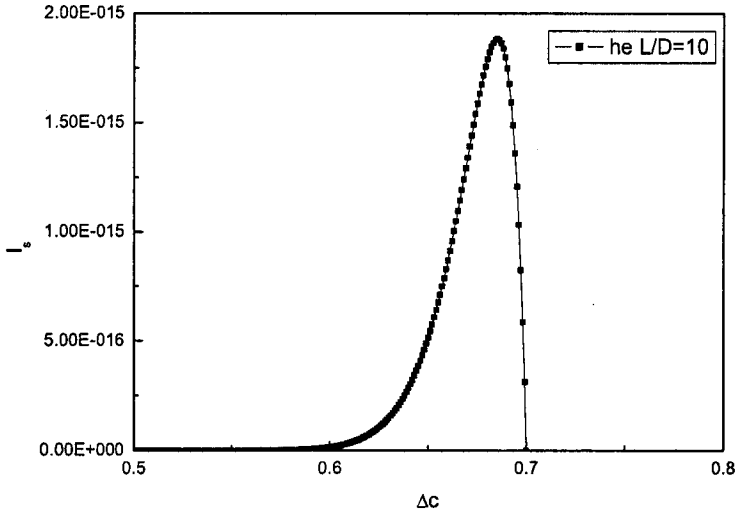


Figure 4.2: Homogeneous elongated droplet with $L/D = 10$, $\omega = 10$.

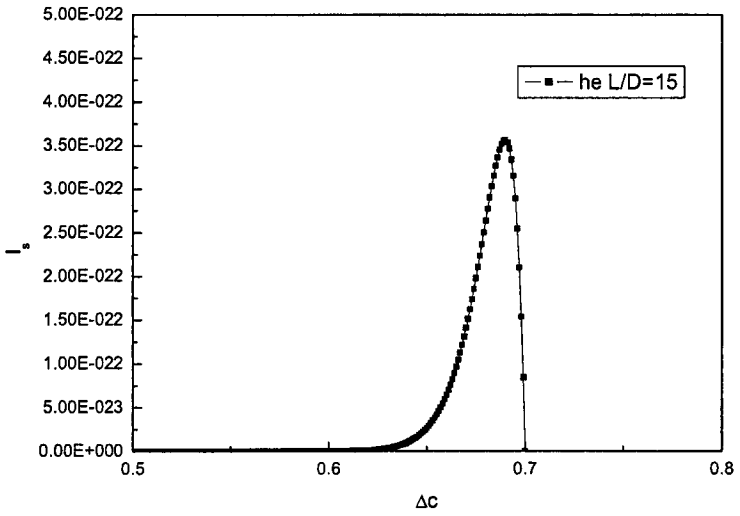


Figure 4.3: Homogeneous elongated droplet with $L/D = 15$, $\omega = 10$.

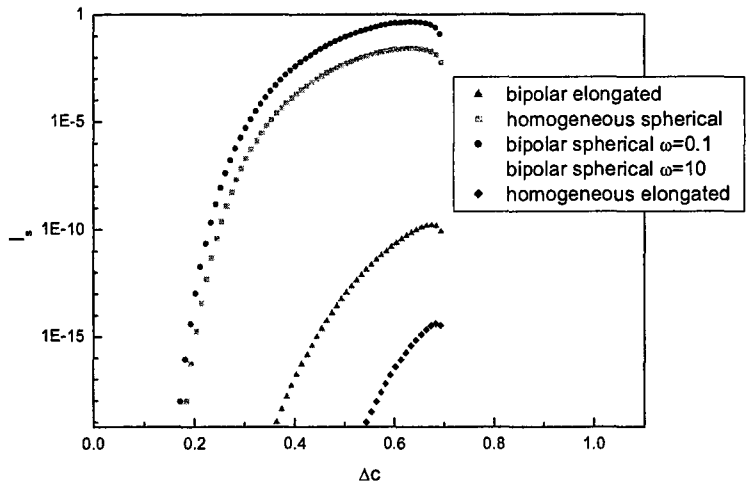


Figure 4.4: Bipolar elongated, homogeneous elongated, homogeneous spherical, bipolar spherical, for bipolar spherical with $\omega = 10$, the dimensionless nucleation rate was found to be below $10^{-200}$ and for the sake of clarity omitted from the graph. $L/D = 10$.

## 4.5 Conclusions

The nucleation rates of all droplet types show a pronounced maximum, as was observed in experiments done with rod-like boehmite particles [2]. The differences between the different droplet types are emphasized by the exponential function of the nucleation rate. One would expect to see the transitions between the different droplet types, as we found for the barriers. From figure 4.4 it can be said that one droplet type (bipolar spherical for $\omega = 0.1$) has a much higher nucleation rate than the others and would therefore always win out. This is inconsistent with what we have seen earlier. Unlike suggested by [2], the decline of the nucleation rate is a result of the slowing down of the orientation fluctuations causing the nucleation rate goes to zero at the spinodal.

# Chapter 5

# Density functional theory

## 5.1 Introduction

In this chapter we discuss an alternative route for calculating the free energy barrier to the formation of a nematic droplet using density functional theory for the case where classical nucleation theory fails (actual calculations are left for future work). This happens for deep quenches close to the spinodal, when the droplet size approaches the particle size. It is then no longer possible to ignore the internal droplet structure. Also, and perhaps more importantly, the capillarity approximation breaks down near the spinodal.

Density functional theory predicts the nucleation barrier to vanish at the spinodal, while classical nucleation theory contains a fundamental inconsistency by predicting a finite barrier despite the fact that the very nature of the spinodal demands the disappearance of this barrier. Another aspect of classical nucleation theory that is questionable for small droplets is the dividing surface that separates the nematic nucleus from the isotropic phase, the physically objective criterion of the actual positioning of this interface remains unclear. [11] Indeed, on approach of the spinodal one expects the interfacial thickness to diverge as the correlation length associated with the orientational fluctuations go to infinity, causing the internal droplet structure to become ramified. [33] [34]

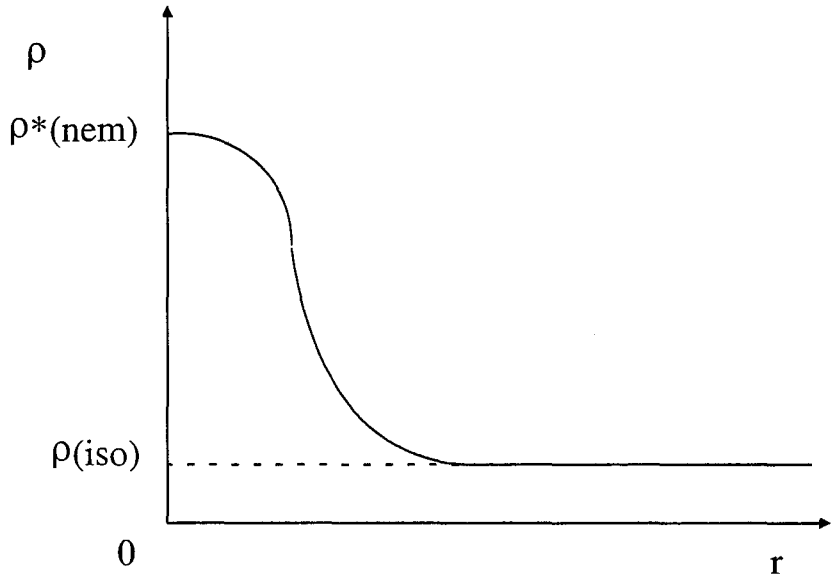


Figure 5.1: density profile for a critical nucleus

Even away from the spinodal, there is a continuous change of the particle number density $\rho$ and orientational parameter through a finite region between the nematic and isotropic phase. In the density functional approach, the free energy is not taken as a function of droplet size but as a functional of the density profile across the interface separating the isotropic phase from the nematic, see figure 5.1. [11] Functional differentiation of the free energy then yields the density profile, and hence the free energy barrier to nucleation. Our aim is to calculate the free energy of a nematic droplet.

Let $\rho(\mathbf{r}, \mathbf{u})$ be the density of the rods with position vector $\mathbf{r}$ of the center of mass and $\mathbf{u}$ the unit vector along the main axis of the rod-like particle. The existence of the spatial inhomogeneity of the molecular density $\rho$ causes the Helmholtz free energy $f$ to be locally different and a function of $(\mathbf{r}, \mathbf{u})$, $\rho$ and its derivatives, which we shall denote as $f(\mathbf{r}, \mathbf{u})$. The Helmholtz free energy $F$ of a system with volume $V$ with can be written as [34] [11]

$$F[\rho] = \int_V f(\mathbf{r}, \mathbf{u})\rho(\mathbf{r}, \mathbf{u}) d\mathbf{r} d\mathbf{u} \tag{5.1}$$

since $\rho(\mathbf{r}, \mathbf{u})d\mathbf{r}d\mathbf{u}$ is the number of particles in the volume $d\mathbf{r}$ around point $\mathbf{r}$ , pointing in the direction of $\mathbf{u}$ (the integration is over the entire volume V of the system). In this way the

Helmholtz free energy $F$ becomes a functional of the particle density $\rho(\mathbf{r}, \mathbf{u})$.

As mentioned earlier, the DFT expression for the Helmholtz free energy contains both an ideal part and an excess part. The excess part is a result of the interaction between a particle with position $\mathbf{r}$ and orientation $\mathbf{u}$ and a particle with position $\mathbf{r}'$ and orientation $\mathbf{u}'$. Accounting for these particle interactions causes great mathematical difficulties and therefore various approximations have been developed. We explore the gradient approximation by similar to that of Cahn and Hilliard [14] [34], which accounts for the dependence of $f$ on $\rho$ and its first derivatives. We apply this theory for a solution of hard rods and account for the non-local interaction between hard rods of finite length. Doi and Kuzuu [15] have calculated the free energy of coexisting, semi-infinite isotropic and nematic bulk phases, separated by a planar interface. Our aim is to calculate the free energy of a finite-sized nematic droplet surrounded by the isotropic bulk phase. Two approaches are considered here, a numerical and an analytical variational approach.

## 5.2 The gradient approximation

The gradient approximation is the pioneering one in the density functional theory of nucleation. It was introduced by Cahn and Hilliard for determining the interfacial energy of a system with non-uniform density [14] and then for analysing nucleation in a two-component incompressible fluids [34]. The assumption is that $f$ is only a function of $\rho$ and its first derivatives and can be approximated as

$$f(\mathbf{r}, \mathbf{u}) = \frac{1}{4\pi} f(\mathbf{r}) = \frac{1}{4\pi} f_u[\rho(\mathbf{r})] + \frac{1}{4\pi} K[\nabla\rho(\mathbf{r})]^2, \tag{5.2}$$

Eq. 5.2 is only valid for spherical particles, here $f_u$ is the Helmholtz free energy (per particle) which the system would have had if it were not only locally (at point $\mathbf{r}$), but everywhere with the same density $\rho$, $K \geq 0$ is a $\rho$-dependent coefficient, and $(\nabla\rho)^2$ is the square gradient of $\rho$. Equation 5.2 is a truncated expansion of $f$ in gradients of $\rho$, and the gradient term describes the departure of the actual energy $f$ at point $\mathbf{r}$ from the energy $f_u$ of a uniformly dense system with density $\rho$. Physically, this term accounts for the interaction of the molecules at point $\mathbf{r}$ with the

other molecules in the system and thus makes $f(\mathbf{r})$ a non-local function of $\mathbf{r}$. The contribution of the gradient term vanishes when $(\nabla\rho)^2 \rightarrow 0$ and since $K$ is positive, this term favours the levelling-off of the density inhomogeneity in the system. [11]

Our aim is to apply Cahn and Hilliard's theory of the square gradient approximation to a solution of rigid rod-like particles in the coexisting isotropic and nematic phase as described by Onsager. Doi and Kuzuu [15] calculated the interfacial tension between an isotropic phase and a nematic phase separated by a planar interface of a lyotropic liquid crystal consisting of rigid rod-like particles. A possible way to calculate the free energy of the nematic droplet is to adapt their method for a droplet. The total free energy of the system is written as [15]

$$\beta F = \int \rho(\mathbf{r},\mathbf{u}) \ln \rho(\mathbf{r},\mathbf{u}) d^2\mathbf{u} d^3\mathbf{r} - \frac{1}{2}\int \rho(\mathbf{r},\mathbf{u})\rho(\mathbf{r}',\mathbf{u}') f_M(\mathbf{r}-\mathbf{r}';\mathbf{u}\mathbf{u}') d^2\mathbf{u}' d^3\mathbf{r}' d^2\mathbf{u} d^3\mathbf{r}, \quad (5.3)$$

where $f_M(\mathbf{r}-\mathbf{r}';\mathbf{u},\mathbf{u}')$ is the Mayer function which equals minus one if two rods with configuration $(\mathbf{r},\mathbf{u})$ and $(\mathbf{r}',\mathbf{u}')$ intersect with each other and zero otherwise. Equation 5.3 includes only the interaction between two particles, which is accurate for slender rods with $L/D >> 1$. Assuming that the spatial variation of $\rho$ is weak, $\rho(\mathbf{r},\mathbf{u})$ can be expanded as

$$\rho(\mathbf{r}',\mathbf{u}') = \rho(\mathbf{r},\mathbf{u}') + (\mathbf{r}-\mathbf{r}')\cdot\nabla\rho(\mathbf{r},\mathbf{u}') + [(\mathbf{r}-\mathbf{r}')\cdot\nabla]^2\rho(\mathbf{r},\mathbf{u}') \quad (5.4)$$

Substituting eq. 5.4 into eq. 5.3 and doing the integral over $\mathbf{r}-\mathbf{r}'$, results in

$$\begin{aligned}\beta F = &\int \rho(\mathbf{r},\mathbf{u}) \ln \rho(\mathbf{r},\mathbf{u}) d^2\mathbf{u} d^3\mathbf{r} + DL^2 \int \rho(\mathbf{r},\mathbf{u})\rho(\mathbf{r},\mathbf{u}')|\mathbf{u}\times\mathbf{u}'| d^2\mathbf{u}' d^2\mathbf{u} d^3\mathbf{r} - \\ &\tfrac{1}{24} DL^4 \int [\nabla\rho(\mathbf{r},\mathbf{u})][\nabla\rho(\mathbf{r},\mathbf{u}')] : (\mathbf{u}\mathbf{u}+\mathbf{u}'\mathbf{u}')|\mathbf{u}\times\mathbf{u}'| d^2\mathbf{u}' d^2\mathbf{u} d^3\mathbf{r},\end{aligned} \quad (5.5)$$

where the second term represents the local excluded volume interaction [16] and the third term represents the spatial inhomogeneity.

A method of finding the equilibrium density profile $\rho(\mathbf{r},\mathbf{u})$ is by functionally minimising eq. 5.3 with respect to the density, which yields the dimensionless chemical potential

$$\frac{\delta\beta F}{\delta\rho} = \mu, \quad (5.6)$$

with $\mu$ the dimensionless chemical potential that conserves mass in the minimisation (it acts like a Lagrangian multiplier). Performing the minimisation gives

$$\rho(\mathbf{r},\mathbf{u}) + 2L^2 D \int \rho(\mathbf{r},\mathbf{u}')|\mathbf{u}\times\mathbf{u}'| d^2\mathbf{u}' + \frac{1}{24} L^4 D \int \nabla\nabla\rho(\mathbf{r},\mathbf{u}) : |\mathbf{u}\times\mathbf{u}'|(\mathbf{u}\mathbf{u}+\mathbf{u}'\mathbf{u}') d^2\mathbf{u} = \mu \quad (5.7)$$

Equation 5.7 can be solved iteratively. The iteration method used by Oxtoby and Evans [35] for the nucleation of the gas to a liquid phase transition can be applied here. A density profile is guessed and substituted into the left-hand side. The chemical potential is then solved for the density at each point, which yields a new density profile. Because the critical nucleus is unstable, it is a saddlepoint [33] [14], not a minimum, of the grand potential causing the iteration to be unstable. If the initial guess is chosen appropriately, the densities will begin to converge upon iteration, but then will eventually diverge away from the stable fixed point. Oxtoby and Evans [35] modified the iteration process to allow for this instability and still permit the determination of the properties of the critical nucleus.

An initial guess is made for the radial droplet profile to have a range parameter, the initial droplet radius $R_i$. For a step profile, for example, $R_i$ is the radius separating the nematic from the isotropic phase. This radius is found by applying classical nucleation theory to calculate the radius of a critical droplet. Starting from this initial guess, eq. 5.7 is iterated. The droplet radius needs to be well chosen, for if $R_i$ is too small the nucleus will shrink, while if $R_i$ is too large the nucleus will grow indefinitely. There is some intermediate value $R_i^*$ which upon iteration will give rise to the critical nucleus, neither growing or shrinking. After a number of calculations, an approximate value for $R_i^*$ is found.

The above method is numerically very demanding because of the extra degrees of freedom, especially for droplets. A relatively quick method is a variational theory, in which the density profile is guessed. This has proven to be quite accurate in practice. The method is analogue to the numerical method, except that the guess is an approximating one.

The variational theory uses a trial function to find $\beta F$ for $\rho(\mathbf{r}, \mathbf{u}) = \nu(\mathbf{r})\psi(\mathbf{r}, \mathbf{u})$ where $\nu$ is the density profile and $\psi$ is the orientational profile. We insert this profile into eq. 5.5 and minimise with respect to the variational parameters. Doi and Kuzuu [15] studied the free energy of coexisting isotropic and nematic phases separated by a planar interface with thickness $\delta$, by extending Onsager's trial function with a density profile as a function of the distance to the interface. Our aim is to use the same trial function, but instead of a planar interface, we

calculate the density profile of the interface separating the nematic droplet from the isotropic. Because of the complexity, we assume the droplet to be spherical with a homogeneous director field. The trial function for the density profile is chosen to be [15]

$$\rho(\mathbf{r},\mathbf{u}) = g(r/\delta)\psi[\alpha(r/\delta)\mathbf{u}\cdot\mathbf{n}], \tag{5.8}$$

where $\delta$ is the interfacial thickness for which we assume to be independent of the angle, $\alpha$ is a variational parameter which is chosen to minimise $\beta F$, and $f(\mathbf{u})$ is the orientational distribution function and chosen by Onsager to be [16]

$$\psi(\mathbf{u}) = \frac{\alpha}{4\pi\sinh(\alpha)}\cosh(\alpha\mathbf{u}\cdot\mathbf{n}), \tag{5.9}$$

where $\mathbf{n}$ is the director. The orientational profile can be written to make Onsager's variational parameter $\alpha$ a function of the radius scaled to the interfacial thickness with the interface positioned at $r = R_*$ [15]

$$\alpha((r-R_*)/\delta) = (\alpha_N/2)[\tanh((r-R_*)/\delta)+1], \tag{5.10}$$

and the density profile $g(r/\delta)$ [15]

$$g((r-R_*)/\delta) = \frac{\rho_N-\rho_I}{2}\tanh((r-R_*)/\delta) + \frac{\rho_N+\rho_I}{2} \tag{5.11}$$

By substituting eq. 5.10 and eq. 5.11 into eq. 5.8 we can calculate the free energy and minimise it with respect to the parameters $\delta$, $\rho_N$ and the droplet radius $R_*$. Eqs. 5.10 and 5.11 are inspired by profiles that accurately describe flat interfaces, so they are suitable for large droplets as for $R_* \to \infty$ the correct flat profile is obtained. Onsager already calculated the first two integrals of eq. 5.5 for the orientational part. The first term (the ideal term) is described as [16]

$$\sigma(\psi) = \int \psi(\mathbf{u})\ln\psi(\mathbf{u})d\mathbf{u}, \tag{5.12}$$

where $\psi$ is the trial function of eq. 5.9. The result in terms of variational parameter $\alpha$ is given as $\sigma(\alpha)$ is [16]

$$\sigma(\alpha) = \ln(\alpha\coth\alpha) - 1 + (\sinh(\alpha))^{-1}\tan^{-1}(\sinh\alpha) \tag{5.13}$$

The second term (the excluded volume term) is described as [16]

$$\rho(\psi) = DL^2 \int \psi(\mathbf{u})\psi(\mathbf{u}')|\mathbf{u} \times \mathbf{u}'|dudu' \tag{5.14}$$

The result of integrating eq. 5.14 over all possible orientations for a monodisperse solution is [16]

$$\rho(\alpha) = \frac{2}{[\sinh(\alpha)]^2} I_2(2\alpha), \tag{5.15}$$

where $I_2$ is a Bessel function of the second order. By calculating the derivatives of eq. 5.15 for a bidisperse solution, which for each different rodlength contains a different $\alpha$, with respect to $\alpha_1$ and $\alpha_2$ (for a monodisperse solution, $\alpha_1 = \alpha_2$) it is possible to calculate the orientational part of the third term of 5.5.

## 5.3 Discussion

Near the spinodal classical nucleation theory can be replaced with density functional theory where the minimisation of the free energy leads to a non-linear integral equation which can in principle be solved numerically. However, since this poses great difficulty for droplets, a variational approach where the Onsager theory for slender rigid rods is expanded seems most promising. In order to simplify the calculations, we have assumed a spherical homogeneous droplet. An expansion for elongated droplets could be made by adding a Legendre polynomial to the profile. In the variational method, the orientational profile of eq. 5.10 is considered to have equal profile as the density profile eq. 5.11. Intuitively this seems incorrect as only the orientational parameter is critical at the spinodal. [5] This may cause a what can be called a para-nematic halo around the nematic droplet, where a region of lower density is part of the critical nucleus. This makes the nematic droplet to be of a completely different structure than described by classical theory.

# Chapter 6

# Conclusions and recommendations

The Laplace pressure contribution to the nucleation barrier is important for deep concentration quenches in a solution containing rod-like particles as long as classical nucleation theory is valid. The Laplace pressure contribution causes the transition between droplet types to shift toward the spinodal. Semi-flexible worms exhibit different behaviour with regard to the Laplace pressure contribution. For theses the Laplace pressure has less impact on the nucleation barrier and the transitions between droplet types are shifted away from the spinodal.

The barrier to nucleation is inversely proportional to the square of the quench depth, causing a deep quench to yield small droplets. For rods the barrier scales as $L/D$ and for worms it scales as $P/D$. The height of the nucleation barrier, and hence the nucleation rate, depends on the surface tension anisotropy, the depth of the concentration quench, and on the elastic properties of the droplets.

The nucleation rate for a solution containing rigid rods has a pronounced maximum and exhibits a slowing down near the suspected spinodal. We suggest that near the spinodal the kinetic prefactor begins to dominate through a hybrid relaxation rate that becomes unstable near the spinodal, causing the critical slowing down of the nucleation dynamics.

The use of interpolation functions between the homogeneous and bipolar droplets should replace the use of the different droplet types found in the asymptotic limit for five regimes.

A variational approach in which the Onsager theory for slender rods is extended for the calculation of the density profile and free energy functional of a critical nucleus seems a promising method for future work.

# Appendix A

# Droplet free energy

## A.1 Laplace pressure contribution

Laplace pressure: $p_n = p + \frac{\partial F}{\partial v} = p + F'$

$$\begin{aligned} G_{ex}(n) &= F(v_n) + 3nkT\left[ln\tfrac{p_n}{p} - (1 - \tfrac{p}{p_n})\right] \\ &= F(v_n) + p_n v_n\left[ln(1 + \tfrac{F}{p}) - \tfrac{F'}{p+F'}\right] \\ &= F(v_n) + \tfrac{1}{2}pV_n\left(\tfrac{F'}{F}\right)^2 \\ G_{ex} &= F + \tfrac{1}{2}pV\left(\tfrac{F'}{p}\right)^2 \end{aligned}$$

Next: calculate $\Delta G = G_{ex} + \rho\Delta\mu V$ for 4 droplet types in both regimes.

Used parameters:

$\tilde{F} = \frac{F}{\tau v^{2/3}}$, $\tilde{\tau} = \tau\xi^2\beta$, $\mathcal{L} = \frac{\tau}{p}\xi^{-1}$, $\tilde{\mu} = \tilde{\rho}\beta\Delta\mu$, $\tilde{\rho} = \rho\xi^3$ and $v = \frac{V}{\xi^3}$.

## A.2 Droplet free energies

- Homogeneous elongated droplets, $\omega \gg 1$

  $\tilde{F} = 6\left(\frac{4\pi}{15}\right)^{1/3}\omega^{1/6}(1 + \frac{1}{21}\omega^{-1} + \dots)$

$F = 6\left(\frac{4\pi}{15}\right)^{1/3}\omega_1\tau\xi^2 v^{2/3}$

$\beta\Delta G = 6\left(\frac{4\pi}{15}\right)^{1/3}\omega_1\tilde{\tau}v^{2/3} + 8\left(\frac{4\pi}{15}\right)^{2/3}\omega_1^2\tilde{\tau}\mathcal{L}v^{1/3} + \tilde{\mu}v$

- Bipolar elongated droplets, $\omega \gg 1$

  $\tilde{F} = \frac{25}{4}\left(\frac{8\pi}{15}\right)^{2/5}\omega^{1/5}v^{-1/15}$

  $F = \frac{25}{4}\left(\frac{8\pi}{15}\right)^{2/5}\omega^{1/5}\tau\xi^2 v^{3/5}$

  $\beta\Delta G = \frac{15}{4}\left(\frac{8\pi}{15}\right)^{2/5}\omega_2\tilde{t}\tilde{a}uv^{3/5}\frac{225}{32}\left(\frac{8\pi}{15}\right)^{4/5}\omega_2^2\tilde{\tau}\mathcal{L}v^{1/5} + \tilde{\mu}v$

- Bipolar spherical droplets, $\omega \gg 1$ and $\omega \ll 1$

  $\tilde{F} = 3\left(\frac{4\pi}{3}\right)^{1/3} + 3\left(\frac{4\pi}{3}\right)^{2/3}(1 + \frac{12-\pi^2}{16}\gamma_{33})\omega v^{-1/3} + \ldots$

  $F = 3\left(\frac{4\pi}{3}\right)^{1/3}\tau\xi^2 v^{2/3} + 3\left(\frac{4\pi}{3}\right)^{2/3}(1 + \frac{12-\pi^2}{16}\gamma_{33})\omega\tau\xi^2 v^{1/3}$

  $\beta\Delta G = 3\left(\frac{4\pi}{3}\right)^{1/3}\tilde{\tau}v^{2/3} + 3\left(\frac{4\pi}{3}\right)^{2/3}\gamma_4\omega\tilde{\tau}v^{1/3} + 2\left(\frac{4\pi}{3}\right)^{2/3}\tilde{\tau}\mathcal{L}v^{1/3} +$

  $\frac{1}{2}\left(\frac{4\pi}{3}\right)^{4/3}\gamma_4^2\omega^2\tilde{\tau}\mathcal{L}v^{-1/3} + 2\left(\frac{4\pi}{3}\right)\omega\gamma_n\tilde{\tau}\mathcal{L} + \tilde{\mu}v$

  $= 2\left(\frac{4\pi}{3}\right)^{1/3}v^{-1/3} + \left(\frac{4\pi}{3}\right)^{2/3}(\gamma_4\omega + \frac{2}{3}\mathcal{L})v^{-2/3} + \frac{\tilde{\mu}}{\tilde{\tau}} - \frac{1}{6}\left(\frac{4\pi}{3}\right)^{4/3}\gamma_4^2\omega^2\mathcal{L}v^{-4/3} = 0$

  - $\omega \gg 1$

    $v \gg \omega^3$ so $v^{-4/3}$ will go to zero fastest. Ignore this term at first and investigate its influence using perturbation theory.

  - $\omega \ll 1$

    $2\left(\frac{4\pi}{3}\right)^{1/3}v^{-1/3} + \left(\frac{4\pi}{3}\right)\gamma_n\omega v^{-2/3} + \frac{2}{3}\left(\frac{4\pi}{3}\right)\mathcal{L}v^{-2/3} - \frac{1}{6}\left(\frac{4\pi}{3}\right)^{4/3}\gamma_n^2\omega^2\mathcal{L}v^{-2/3} + \frac{\tilde{\mu}}{\tilde{\tau}} = 0$

    Choose $\omega = 0.1$, $\gamma_n = \left(1 + \frac{12-\pi^2}{16}\gamma_{33}\right)$

    $\mathcal{L} \sim \omega$, so for $\omega \ll 1$, $\mathcal{L}$ is small.

    1. Neglect $\gamma_n\omega\mathcal{L}$
    2. Neglect $(\gamma_n\omega)^2$
    3. Neglect $\mathcal{L}^2$

- Homogeneous spherical droplets, $\omega \ll 1$

  $\tilde{F} = 3\left(\frac{4\pi}{3}\right)^{1/3}\left(1 + \frac{1}{3}\omega - \frac{\pi^2}{36(\pi^2-8)}\omega^2 + \ldots\right)$

$$F = 3\left(\tfrac{4\pi}{3}\right)^{1/3}\omega_3\tau\xi^2 v^{2/3}$$
$$\beta\Delta G = 3\left(\tfrac{4\pi}{3}\right)^{1/3}\omega_3\tilde{\tau}v^{2/3} + 2\left(\tfrac{4\pi}{3}\right)^{2/3}\omega_3^2\tilde{\tau}\mathcal{L}v^{1/3} + \tilde{\mu}v$$

# Bibliography


[1] P.G. Debenedetti. *Metastable liquids.* Princeton University press, Princeton, 1 edition, 1996.

[2] M.P.B. van Bruggen, J.K.G. Dhont, and H.N.W. Lekkerkerker. Morphology and kinetics of the isotropic and nematic phase transition in a dispersion of hard rods. *Macromolecules*, 32:2256, 1999.

[3] N.M. Dixit and C.F. Zukoski. Kinetics of crystallization in hard-sphere colloidal suspensions. *Physical Review E*, 64:041604–1, 2001.

[4] B.J. Ackerson and K. Schatzel. Classical growth ot hard-sphere colloidal crystals. *Physical Review E*, 52:6448, 1995.

[5] J.W. Winters, T. Odijk, and P. van der Schoot. spinodal decomposition in a semidilute suspension of rodlike macromolecules. *Physical Review E*, 63:011501–1, 2000.

[6] P. Prinsen. de vorm van een nematische druppel vloeibare kristal in een vloeibare isotrope fase, 2002.

[7] G.J. Vroege en H.N.W. Lekkerkerker. Phase transitions in lyotropic colloidal and polymer liquid crystals. *Reports of Progress in Physics*, 55:1241–1309.

[8] P. Prinsen and P. van der Schoot. Continous director field transformation of nematic tactoids. *preprint*, 2003.

[9] P. Prinsen and P. van der Schoot. Shape and director field transformation of tactoids. *Physical Review E*, 68:021701, 2003.

[10] J. Rudnick and R. Bruinsma. *Physical Review Letters*, 74:2491, 1995.

[11] D. Kaschiev. *Nucleation basic theory and applications.* Butterworth Heineman, Oxford, 2000.

[12] K.F. Kelton. crystal nucleation in liquids and gases. *Solid state physics*, 45:75–177, 1991.

[13] S.A. Auer. *Quantitative Prediction of Crystal Nucleation Rates for Spherical Colloids: a Computational Study.* PhD thesis, 2002.

[14] Cahn and Hilliard. Free energy of a nonuniform system i interfacial free energy. *Journal of Chemical Physics*, 28:258, 1958.

[15] Doi and Kuzuu. Structure of the interface between the nematic phase and the isotropic phase in the rodlike molecules. *Journal of applied polymer science: applied polymer symposium*, 41:65, 1985.

[16] L. Onsager. The effects of shape on the interaction of colloidal particles. *Annals of New York Acadademy of Sciences*, 51:627–659, 1949.

[17]

[18] David Boal. *Mechanics of the Cell.* Cambridge University press, Cambridge, 2002.

[19] P.A.Janmey, J.X. Tang, and C.F.Schmidt. Actin filaments.

[20] J.X.Tang, R. Oldenburg, P.G.Allen, and P. Janmey.

[21] R.F.Schmidt and G.Thews. *human physiology.* Springer, Berlin, 1989.

[22] R.W. Briehl R.E. Samuel, E.D. Salmon. Nucleation and growth of fibres and gel formation in sickle cell hemoglobin. *Nature*, 345:833, 1990.

[23] P.G. De Gennes and J. Prost. *The physics of liquid crystals.* Clarendon, Oxford, 1993.

[24] T. Odijk. Theory of lyotropic polymer liquid crystals. *Macromolecules*, 19:2313, 1986.

[25] P. van der Schoot. Remarks on the interfacial tension in colloidal systems. *Journal of Physical Chemistry B*, 103:8804–8808, 1999.

[26] T. Sato and A. Teramoto. On the frank elastic constants of lyotropic polymer liquid crystals. *Macromolecules*, 29:4107–4114, 1996.

[27] T. Odijk. Elastic constants of nematic solutions of rodlike and semiflexible polymers. *Liquid Crystals*, 1:553, 1986.

[28] S. Cui, O. Akcakir, and Z.Y. Chen. Isotropic-nematic interface of liquid-crystalline polymers. *Physical Review E*, 51:4548, 1995.

[29] A.Y. Grosberg and A.V. Zhestkov. The dependence of the elasticity coefficients of a nematic liquid crystal on macromolecular rigidity. *Polymer Science U.S.S.R*, 28:97–104, 1986.

[30] D.W. Oxtoby. Homogeneous nucleation:theory and experiment. *Journal of physics: Condensed Matter*, 4:7627–7650, 1992.

[31] K.F. Kelton. Transient nucleation in condensed systems. *Journal of Chemical Physics*, 79:6261–6276, 1983.

[32] S.Glasstone, K.J.Laidler, and H.Eyring. *The theory of rate process.* McGraw-Hill, New York and London, 1941.

[33] W. Klein and C. Unger. Pseudospinodals, spinodals and nucleation. *Physical Review B*, 28:445.

[34] Cahn and Hilliard. Free energy of a nonuniform system iii nucleation in a two component incompressible fluid. *Journal of Chemical Physics*, 31:688, 1959.

[35] D.W. Oxtoby and R. Evans. Nonclassical nucleation theory for the gas-liquid transition. *Journal of Chemistry and Physics*, 89:7521, 1988.